International Journal of Heat and Mass Transfer 80 (2015) 469–493

Contents lists available at ScienceDirect

International Journal of Heat and Mass Transfer

journal homepage: www.elsevier.com/locate/ijhmt

Review

# Review of flow boiling and critical heat flux in microgravity

Christopher Konishi, Issam Mudawar *

*Purdue University Boiling and Two-Phase Flow Laboratory (PU-BTPFL), School of Mechanical Engineering, 585 Purdue Mall, West Lafayette, IN 47907, USA*

ARTICLE INFO

*Article history:*
Received 10 July 2014
Received in revised form 4 September 2014
Accepted 8 September 2014
Available online 11 October 2014

*Keywords:*
Flow boiling
Critical heat flux
Reduced gravity
Microgravity

ABSTRACT

Space agencies worldwide are actively exploring the implementation of two-phase thermal management systems to support astronaut life onboard future space vehicles and planetary bases. Key motivations for these efforts are to increase the efficiency of power utilization and reduce overall weight and volume. These advantages are realized by orders of magnitude enhancement in heat transfer coefficient achieved with flow boiling and condensation compared to single-phase systems. This study will review published literature concerning two-phase flow and heat transfer in reduced gravity. Discussed are the different methods and platforms dedicated to exploring the influence of reduced gravity, including ground flow boiling experiments performed at different orientations relative to Earth gravity, as well as reduced gravity adiabatic two-phase flow, pool boiling, flow boiling and CHF experiments. Despite the extensive data and flow visualization results available in the literature, it is shown that there is a severe shortage of useful correlations, mechanistic models and computational models, which compromises readiness to adopt flow boiling in future space systems. Key recommendations are provided concerning platform, heater design, and operating conditions for future studies to expedite the deployment of two-phase thermal management in future space missions.



**Contents**



* Corresponding author. Tel.: +1 (765) 494 5705; fax: +1 (765) 494 0539.
*E-mail address:* mudawar@ecn.purdue.edu (I. Mudawar).
*URL:* https://engineering.purdue.edu/BTPFL (I. Mudawar).

http://dx.doi.org/10.1016/j.ijheatmasstransfer.2014.09.017
0017-9310/

**Nomenclature**

| | |
|---|---|
| $A$ | cross-sectional area of flow channel |
| $b$ | ratio of wetting front length to wavelength |
| $Bo$ | Bond number |
| $C_{f,i}$ | interfacial friction coefficient |
| $C_o$ | distribution parameter in Drift Flux model |
| $c_p$ | specific heat at constant pressure |
| $D$ | diameter |
| $D_h$ | hydraulic diameter, $4A/P$ |
| $f$ | friction factor |
| $Fr$ | Froude number |
| $G$ | mass velocity |
| $g$ | gravity |
| $g_e$ | Earth gravity |
| $g_n$ | component of gravity normal to heated wall |
| $g_{//}$ | component of gravity opposite to direction of fluid flow |
| $H$ | height of channel's cross-section |
| $h$ | heat transfer coefficient |
| $H_f$ | mean thickness of liquid layer |
| $h_{fg}$ | latent heat of vaporization |
| $H_g$ | mean thickness of vapor layer |
| $j$ | superficial velocity |
| $k$ | thermal conductivity; wave number ($2\pi/\lambda$) |
| $L$ | heated length |
| $\dot{m}$ | mass flow rate |
| $Nu$ | Nusselt number |
| $P$ | perimeter |
| $p$ | pressure |
| $Pr$ | Prandtl number |
| $Q$ | volumetric flow rate |
| $q''$ | wall heat flux |
| $q''_m$ | critical heat flux (CHF) |
| $q''_w$ | wetting front lift-off heat flux |
| $Re$ | Reynolds number |
| $T$ | temperature |
| $\Delta T_{sub,o}$ | outlet subcooling, $T_{sat,o} - T_{b,o}$ |
| $U$ | mean liquid inlet velocity |
| $U_f$ | mean velocity of liquid layer |
| $U_g$ | mean velocity of vapor layer |
| $U_{g,n}$ | mean vapor velocity in wetting front normal to heated wall |
| $U_\infty$ | bubble rise velocity |
| $W$ | heated width of channel's cross-section |
| $We$ | Weber number |
| $x_e$ | thermodynamic equilibrium quality |
| $z$ | stream-wise coordinate |
| $z_o$ | distance from leading edge of heated wall to location where vapor velocity surpasses liquid velocity |

*Greek symbols*

| | |
|---|---|
| $\alpha$ | vapor void fraction |
| $\delta$ | mean thickness of vapor layer |
| $\delta_h$ | heated wall thickness |
| $\eta$ | interfacial perturbation |
| $\eta_o$ | amplitude of interfacial perturbation |
| $\lambda$ | wavelength |
| $\lambda_c$ | critical wavelength |
| $\mu$ | dynamic viscosity |
| $\nu$ | kinematic viscosity |
| $\Pi$ | dimensionless group |
| $\rho$ | density |
| $\rho''$ | modified density |
| $\sigma$ | surface tension |
| $\tau$ | shear stress |
| $\theta$ | flow orientation angle |

*Subscripts*

| | |
|---|---|
| *asymp* | asymptotic |
| *b* | bulk liquid |
| *f* | saturated liquid |
| *g* | saturated vapor |
| *h* | heated wall |
| *i* | interface |
| *in* | inlet to heated wall |
| *m* | critical heat flux |
| *min* | minimum |
| *max* | maximum |
| *o* | outlet from heated wall |
| *sat* | saturation |
| *sub* | subcooling |
| *w* | wetting front; heated wall |

## 1. Introduction

### 1.1. Importance of two-phase thermal management to future space missions

Many modern applications requiring the dissipation of large concentrated heat loads rely on two-phase thermal management systems that employ both flow boiling and condensation. Unlike single-phase systems, which rely entirely on sensible heat rise of the working fluid to remove the heat, two-phase systems capitalize upon latent heat in addition to the sensible heat, which allows them to achieve orders of magnitude enhancement in heat transfer coefficient and much lower temperatures of the heat dissipating device compared to single-phase counterparts [1]. Associated with heat-flux controlled flow boiling, critical heat flux (CHF) is arguably the most important design parameter for two-phase thermal management systems. Since exceeding this limit can lead to catastrophic failure, a key goal in designing a two-phase thermal management system is to increase CHF in order to broaden the useful nucleate boiling heat flux range. This important goal has spurred many recent research efforts to both increase and predict CHF using a variety of boiling configurations, including pool [2,3], channel flow [4,5], mini/micro-channel [6], spray [7,8], and jet [9–11], as well as hybrid cooling configurations [12,13].

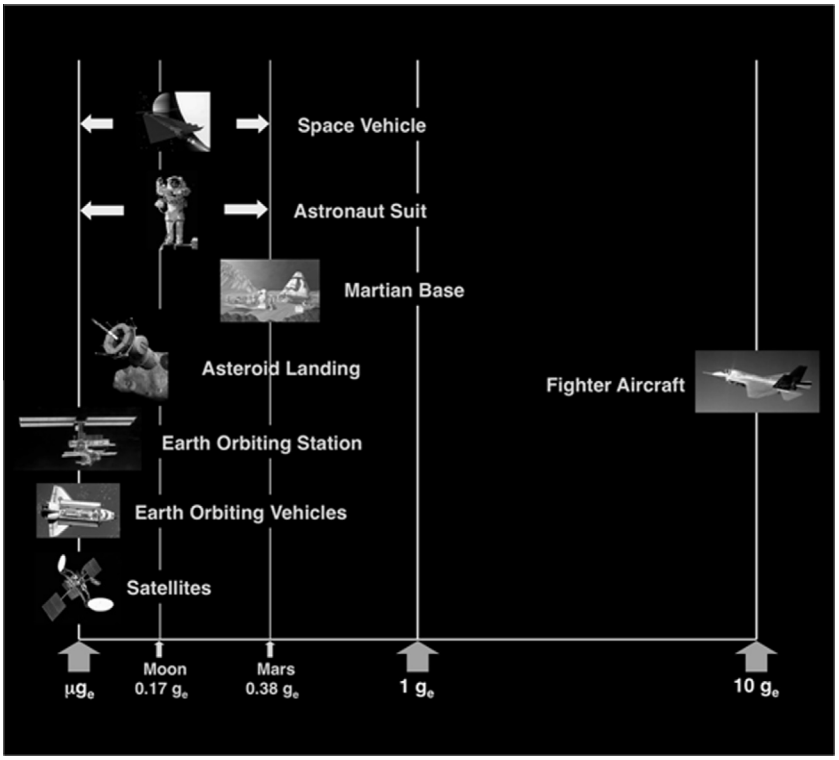


**Fig. 1.** Examples of space systems demanding predictive models of the effects of gravity on two-phase flow and heat transfer.

Space agencies worldwide are presently exploring the implementation of two-phase thermal management systems to support astronaut life onboard future space vehicles and planetary bases. Key motivations for these efforts are to increase the efficiency of power utilization, and reduce overall weight and volume; these attributes are direct benefits of the heat transfer enhancement achieved with flow boiling and condensation. Prime examples of these space systems are NASA's Fission Power System (FPS), which can deliver both very high power and very low mass to power ratio, and Thermal Control Systems (TCSs), which are responsible for controlling the temperature and humidity of the operating environment in a space vehicle or planetary base [14,15]. A key challenge in designing these systems is that they must endure varying gravitational fields as depicted in Fig. 1, rather than microgravity alone. Understanding the influence of different gravitational environments on two-phase fluid physics and heat transfer is therefore crucial to the development of these systems.

The influence of gravity on flow boiling is reflected in buoyancy, which is proportional to the product of gravity and density difference between liquid and vapor. Because of the large density difference, buoyancy can play an important role in dictating the motion of vapor relative to liquid and therefore influence heat transfer effectiveness. Buoyancy can also have a drastic effect on flow boiling CHF. Operating in the nucleate boiling region below CHF enables the attainment of both high nucleate boiling heat transfer coefficients and low surface temperatures. However, intense vapor production can lead to appreciable vapor coalescence along the wall, which resists liquid access to the wall. CHF occurs when the liquid replenishment is interrupted, and is manifest by an unsteady rise in the wall temperature.

Unfortunately, most of the two-phase fluid flow and heat transfer know-how amassed over nearly a century of research comes from experiments that were conducted in Earth's gravity. High cost, hardware complexity, and sparse data that researchers are able to obtain from short-duration microgravity experiments, compounded by limited access to testing in orbiting stations, are all reasons behind the relatively small body of literature on two-phase transport phenomena in reduced gravity.

### 1.2. Microgravity testing platforms

Performing boiling experiments in reduced gravity, especially microgravity, is a challenging and costly endeavor. Several types of testing platforms have been used for this purpose. Microgravity can be achieved by placing an experimental package in a state of freefall in an above ground *drop tower* or below ground *drop shaft*. These platforms provide high quality microgravity ($<1 \times 10^{-4}$ $g_e$) for relatively short durations between 2.2 and 10 s (2.2 s for NASA Glenn Research Center's 24-m drop tower, 5.2 s for NASA Glenn Research Center's 132-m drop shaft, 4.6 s for NASA Marshall Space Flight Center's 105-m drop tower, 4.72 s for Germany Drop Tower Bremen's (ZARM's) 110-m drop tower, and 10 s for Japan Microgravity Center's (JAMIC's) 700-m drop shaft) [16]. Key disadvantages of drop towers and drop shafts are (1) inability to reach steady-state for many types of experiments because of the short test duration, (2) need to perform many repetitive drops to acquire sufficient data (since only one set of operating conditions can be tested in a single drop), and (3) inability to interact manually with the experimental package during the drop. Due to short microgravity duration and low operational cost, drop towers and shafts are primarily used for initial validation of experiments before more comprehensive testing is carried out on long-duration microgravity platforms.

Sounding rockets provide another platform to achieving microgravity during a sub-orbital flight. They provide 3–13 min of testing with high quality microgravity ($<1 \times 10^{-4}$ $g_e$) [16]. Sounding rockets share the disadvantages of drop towers and shafts in their inability to interact with the experimental package, or to perform multiple experiments at different operating conditions; they also cannot accommodate large experimental packages.

Parabolic flight aircraft provide a cost effective means to achieving microgravity with durations of 15–30 s. Through a series of parabolic maneuvers, varying gravitational conditions can be

achieved, including microgravity ($\mu g_e$), Lunar gravity and Martian gravity. Parabolic flight experiments offer considerable advantages over drop towers and drop shafts and sounding rockets, including ability to (1) accommodate larger experimental packages, (2) test many different operating conditions in multiple parabolas during the same flight, and (3) grant the experimenter manual access to the facility. Their key drawback is relatively low quality microgravity (±0.01 $g_e$) and '*g-jitter*,' which are influenced by pilot skills and weather related turbulence [16].

A few studies were privileged use of NASA's Space Shuttles for microgravity experimentation. During their active years, Space Shuttles satisfied virtually all testing needs, including (1) ability to perform long duration experiments, (2) high quality microgravity ($<1\times10^{-4}\ g_e$), (3) operator access to the experimental package, and (4) both automatic and remote control capabilities. However, the process of granting testing onboard Space Shuttles required long periods of development and safety certification, let alone the very high cost.

With the retirement of NASA's Space Shuttle program, the International Space Station (ISS) presently provides the ultimate testing environment for microgravity research, sharing benefits similar to those of the Space Shuttles [17]. But like Space Shuttle experiments, ISS experiments are very costly and require many years of development and safety certification. These drawbacks pose major obstacles to meeting researchers' needs for microgravity flow boiling data.

### 1.3. Transition from pool boiling to flow boiling in microgravity

The vast majority of microgravity boiling research performed to date has been focused on pool boiling. The original intent in pool boiling studies was to develop fundamental understanding of the influence of microgravity on such phenomena as boiling incipience, bubble nucleation, growth and coalescence, nucleate boiling heat transfer, and, most importantly, CHF [14]. Spanning over 60 years, most of these studies point to the danger of enormous bubble growth because of the absence of an effective force to remove the bubble from the heated wall. This also points to the danger of abrupt occurrence of CHF at relatively low heat fluxes. These complications render the implementation of pool boiling in space systems very impractical.

Recently, there have been urgent calls to shift the focus of microgravity research from pool boiling to flow boiling in order to achieve both the high heat transfer coefficients and high CHF values required for space applications [14,15]. In the absence of a body force to remove vapor bubbles from the boiling wall, flow boiling can augment CHF in microgravity by relying on bulk liquid motion to flush bubbles away before they coalesce into large insulating vapor masses, and to replenish the wall with bulk liquid. Despite these highly acknowledged merits of flow boiling, very few microgravity flow boiling experiments have been performed to date. This can be attributed to the high complexity and high cost of flow boiling microgravity test facilities compared to those intended for pool boiling. Flow boiling facilities are typically much larger, include many more components, and demand greater power. They also require a longer microgravity test duration to achieve steady state, which makes them difficult to implement in drop towers, drop shafts, sounding rockets and parabolic flight aircraft.

### 1.4. Predictive tools for flow boiling CHF at one $g_e$

#### 1.4.1. CHF types

Although there is much debate concerning the precise mechanism for flow boiling CHF, researchers concur that, for heat-flux-controlled systems, this phenomenon is associated with a sharp rise in wall temperature and drastic reduction in the local heat transfer coefficient resulting from inadequate liquid access to the wall. Two different terms that are commonly used to describe CHF are *Dryout* and *Departure from Nucleate Boiling* (*DNB*). Dryout typically occurs in high quality flows exhibiting annular flow boiling, where the annular liquid film is progressively consumed by evaporation along the tube. The term 'dryout' is used to describe the complete evaporation of the liquid film as the cause for CHF. DNB is more prevalent with subcooled inlet conditions and higher mass velocities, and is typically encountered in the bubbly flow regime. Here, substantial heat input causes loss of liquid access to the heated wall despite the presence of adequate bulk liquid elsewhere within the channel. In general, dryout is a milder form of CHF, encountered at relatively lower heat fluxes and causes moderate wall temperature excursions. DNB, on the other hand, is associated with much higher heat fluxes, and precipitates large and rapid temperature excursions. It is therefore the more dangerous form of CHF and poses the greater potential for physical damage to the heated wall.

#### 1.4.2. CHF empirical correlations

Accurate predictive tools for flow boiling CHF are vital to the design of a two-phase thermal management system. Studies dedicated to understanding and predicting flow boiling CHF date back to the 1940s. Published literature includes numerous CHF databases and empirical correlations for specific fluids, flow geometries and operating conditions. But unlike single-phase correlations, flow boiling CHF correlations often provide inaccurate predictions. The following comparison provides a simple reason for this limitation.

Consider the Dittus–Boelter correlation for turbulent flow in a heated tube [18],

$$Nu=\frac{hD}{k_f}=0.023Re^{0.8}Pr^{0.4}\begin{cases}Re>10,000\\0.6<Pr<160\end{cases}. \tag{1}$$

This correlation consists of a single dimensionless group, *Nu*, presented as a function of only two independent dimensionless groups, *Re* and *Pr*. The range of $Re>10{,}000$ encompasses very broad ranges of flow rates and fluid properties. And, excepting liquid metals and highly viscous fluids, the Prandtl number range of 0.6–160 covers numerous types of fluids, including both liquids and gases. These attributes explain the popularity of Eq. (1) as a highly effective broad-bases design tool.

Let us now consider a typical correlation for flow boiling CHF in tubes [19],

$$\frac{q''_m}{Gh_{fg}}=f\left(\frac{\rho_f}{\rho_g},\frac{G^2L}{\sigma\rho_f},\frac{C_{p,f}\Delta T_{sub}}{h_{fg}},\frac{L}{D},\frac{G}{\rho_f\sqrt{g_eD}},..\right)=f(\Pi_1,\Pi_2,\Pi_3,\Pi_4,\Pi_5,..)\begin{cases}\Pi_{1,min}<\Pi_1<\Pi_{1,max}\\\Pi_{2,min}<\Pi_2<\Pi_{2,max}\\\Pi_{3,min}<\Pi_3<\Pi_{3,max}\\\Pi_{4,min}<\Pi_4<\Pi_{4,max}\\\Pi_{5,min}<\Pi_5<\Pi_{5,max}\end{cases}. \tag{2}$$

Unlike Eq. (1), this CHF correlation (a) is a function of numerous independent dimensionless groups, and (b) each of the independent groups is valid over a finite range. Given the high cost of conducting two-phase experiments compared to their single-phase counterparts, the ranges of individual independent parameters are usually quite small. This limits the usefulness of the CHF correlation to relatively narrow ranges of many independent parameters, and the correlation is therefore valid over a very small region of the multidimensional space encompassing all the independent parameters. Additionally, extrapolations to parameter ranges outside those for which the correlation is developed can lead to highly inaccurate predictions.

#### 1.4.3. CHF models

An alternative to empirical CHF correlations is to develop mechanistic theoretical models based on a postulated or visually confirmed CHF trigger mechanism. Most models have been developed specifically for vertical upflow at one $g_e$, which the orientation most commonly adopted and provides stable two-phase flow. Illustrated in Fig. 2, four main mechanisms have been proposed to initiate flow boiling CHF: *Boundary Layer Separation*, *Bubble Crowding*, *Sublayer Dryout*, and *Interfacial Lift-Off*. The Boundary Layer Separation Model [20,21] utilizes analogy between wall gas injection – transpiration – into a single-phase liquid boundary layer and vapor effusion at a heated wall in flow boiling. In the case of single-phase flow, wall injection decreases the liquid velocity gradient near the wall. Ultimately, the gradient becomes vanishingly small once the injection velocity reaches a threshold value, causing the boundary layer to separate from the wall. By analogy, the Boundary Layer Separation Model is based on the premise that CHF occurs when the rate of vapor effusion normal to the heated wall reaches a threshold value that causes appreciable reduction in the bulk liquid velocity gradient, and eventual separation of the liquid from the wall. The Bubble Crowding Model [22,23] is based on the premise that CHF occurs when accumulation of oblong bubbles along the heated wall becomes too dense to permit turbulent fluctuations in the core liquid to provide adequate liquid supply to the wall. The Sublayer Dryout Model [24] is based on the premise that as CHF is approached, oblong bubbles propagating along the heated wall trap thin liquid sublayers. CHF is postulated to occur when heat supplied at the wall exceeds the enthalpy of bulk liquid replenishment of the sublayer. The Interfacial Lift-off Model [25–28] is based on the observation that, prior to CHF, vapor patches generated along the heated wall coalesce into a fairly continuous wavy vapor layer. The wavy interface is able to maintain contact with the wall in 'wetting fronts' corresponding to the wave troughs. CHF is postulated to occur when intense evaporation of liquid in the wetting fronts causes the wavy interface to be lifted off the wall, extinguishing any further liquid replenishment.

#### 1.5. Differences in methods of measuring flow boiling CHF, and importance of heated wall design

Developing reliable CHF correlations and models requires systematic and consistent methods for CHF detection and measurement. Surprisingly, there is great uncertainty in the heat transfer community concerning the precise definition of CHF, evidenced by differences in the experimental methods adopted for CHF detection [29,30], and these differences can lead to significant differences in the measured CHF [31]. The most popular methods for CHF detection can be summarized as follows: (a) first measurable degradation in flow boiling heat transfer, indicated by a slope change of the upper portion of the nucleate boiling region of the boiling curve [32–34], (b) a rise in heated wall temperature above a fixed level designated by the experimenter [35,36], followed by either manual or automatic shut-off of the heat supply, (c) appreciable unsteady temperature rise of any portion of the heated wall [37,38], and (d) allowing sufficient, albeit short period of time for the heated wall to recover from any brief localized temperature excursion, then increasing the heat flux further until the wall temperature escalates uncontrollably [39].

Konishi et al. [40] discovered first-hand instances of localized premature dryout before true CHF occurrence in their experimental study of flow boiling CHF in a rectangular channel subjected to one-sided heating. Fig. 3(a) shows temporal records of the heated wall thermocouples ($T_1$–$T_5$), heat transfer coefficients at the same axial locations as the thermocouples, and wall heat flux for $G/\rho_f = 0.224$ m/s, inlet quality of $x_{e,in} = 0.01$, and channel orientation of $\theta = 315°$ (measured counterclockwise from horizontal orientation of $\theta = 0°$). Notice the momentary dryout detected at upstream thermocouple $T_1$ and, to a lesser extent $T_2$, after the wall heat flux is increased by a small increment then held constant. Remarkably, without increasing the heat flux, $T_1$ begins to level off and decrease slightly before returning to steady state. Testing proceeded by increasing heat input in several small increments, each followed by an adequate waiting period, and all the wall temperatures increased gradually to new steady state levels with no spikes. Eventually, CHF was detected near the outlet of the heated wall by a sudden uncontrolled temperature rise commencing at $T_5$ and $T_4$ with no signs of temperature recovery. These findings point

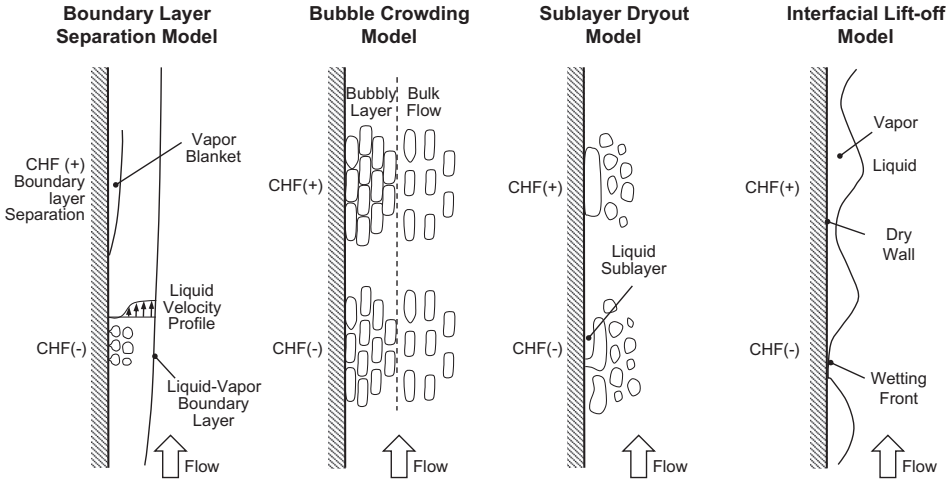


**Fig. 2.** Trigger mechanisms for flow boiling CHF according to different models.

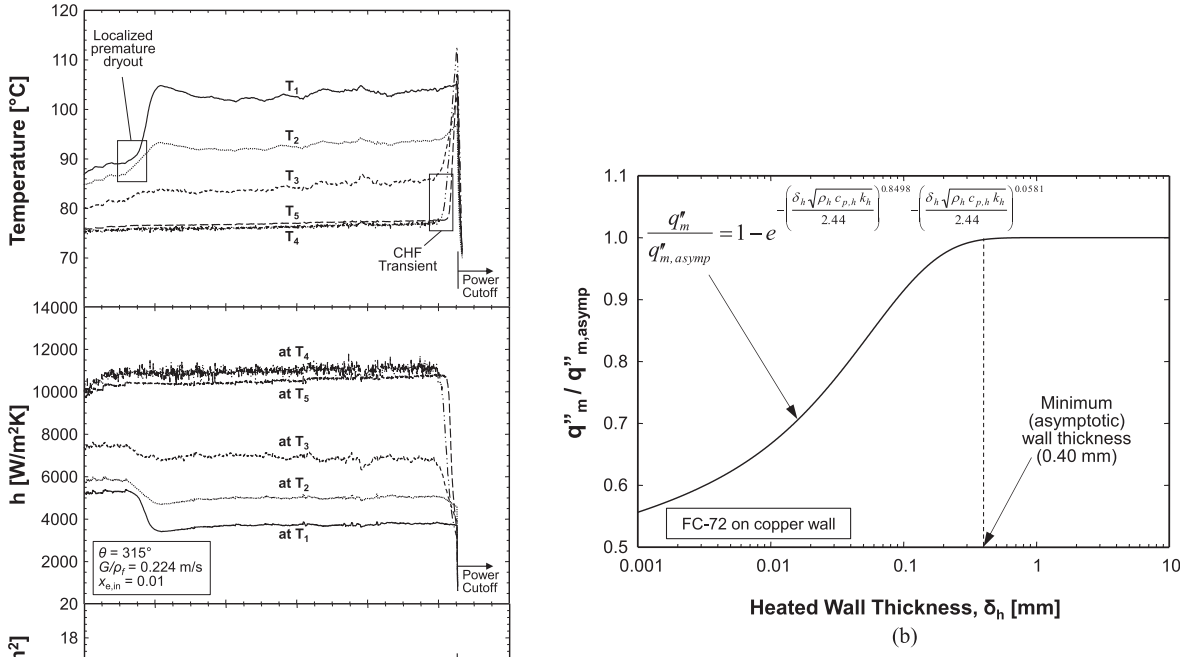


**Fig. 3.** (a) Temporal records of wall temperatures, heat transfer coefficients and wall heat flux for inclined flow boiling of FC-72 [40]. (b) Effect of wall thickness on CHF, and determination of minimum wall thickness required to yield CHF values representative of those of metallic walls of practical interest [42].

to potential errors when interpreting premature localized dryout as true CHF.

Another source of error in CHF detection and measurement is improper design of the heated wall. Guglielmini and Nannei [41] showed that CHF magnitude can be greatly influenced by the wall thickness, $\delta_h$, and thermal properties ($k_h$, $\rho_h$, $c_{p,h}$) of the heated wall. Zhang et al. [42] examined these influences to determine a sufficient wall thickness for their copper heated wall. Fig. 3(b) shows the variation of CHF for FC-72 with wall thickness. Notice how a very thin wall can produce unusually small CHF values. However, by exceeding a thickness of 0.4 mm, an asymptotic CHF value is reached. Therefore, it is imperative to employ a wall thickness for CHF measurement that is within the asymptotic range. As discussed later, some investigators have used heating walls consisting of a semi-transparent gold film that is sputtered onto a glass wall for CHF measurement to achieve wall transparency and optical access [43]. This type of construction generally provides wall thicknesses that are far smaller than the required minimum asymptotic value.

### 1.6. Objectives of study

This study will review published literature concerning two-phase flow and heat transfer in reduced gravity. This encompasses the different methods and platforms dedicated to exploring the influence of reduced gravity, including ground flow boiling experiments performed at different orientations relative to Earth gravity, as well as adiabatic two-phase flow, pool boiling, flow boiling and CHF reduced gravity experiments. Discussed in this review are key mechanisms, correlations and models from these studies, as well as implementation of the same tools in design of thermal management systems in future space missions.

## 2. Terrestrial studies on influence of body force on flow boiling CHF

### 2.1. Method for achieving reduced component of gravity perpendicular to heated wall

A common method to simulating reduced gravity in terrestrial experiments is boiling on a heated wall that is tilted relative to Earth gravity. This provides a partial component of gravity perpendicular to the heated wall. However, a fundamental weakness to this approach is the inability to achieve true reduced gravity since tilting the heated wall also results in a finite component of gravity parallel to the wall. Nonetheless, terrestrial boiling experiments are far less expensive than microgravity counterparts, and provide valuable insight into the CHF mechanism.

### 2.2. Influence of heated wall orientation on pool boiling

Class et al. [44], Githinji and Sabersky [45], Marcus and Dropkin [46], Chen [47], Nishikawa et al. [48], and Kumar et al. [49] examined the influence of wall orientation on pool boiling. These studies demonstrated both drastic variations of CHF value and vast differences in CHF trigger mechanism with orientation, which implies that different CHF models must be pursued for the different orientations. Interestingly, these studies also prove that the classical pool boiling CHF model by Zuber et al. [50] is valid only for horizontal or near-horizontal upward-facing orientations. The strong influence of

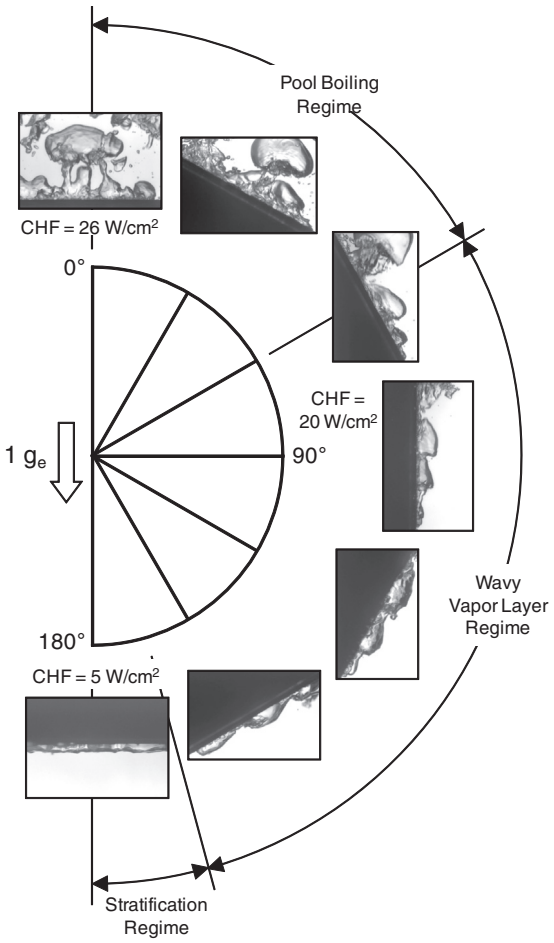


**Fig. 4.** CHF regimes for saturated pool boiling of PF-5052 on a $1.27 \times 1.27$ cm$^2$ heated wall at different orientations [52].

orientation on pool boiling CHF is also evident from studies by Mudawar et al. [51] and Howard and Mudawar [52], who conducted extensive measurements and photographic studies of interfacial behavior for different orientations. Overall, they divided pool boiling wall orientation effects into three regions: near-horizontal upward-facing, near-vertical, and downward-facing as depicted in Fig. 4. In the near-horizontal upward-facing region, buoyancy forces were observed to remove the vapor vertically off the heated wall in accordance with the Zuber et al. model. The near-vertical orientations produced a wavy vapor layer that swept along the heater wall, closely resembling the Interfacial Lift-off mechanism for vertical flow boiling CHF illustrated in Fig. 2. The downward-facing wall orientations caused the vapor to stratify on the heated wall, greatly reducing CHF relative to all other orientations.

### 2.3. Influence of flow and heated wall orientations on flow boiling CHF

Several terrestrial studies were also conducted to explore flow boiling CHF for different orientations. These studies point to orientations effects far more complex that those for pool boiling because of the strong influence of velocity. Simoneau and Simon [53] showed that vapor motion in vertical nitrogen downflow changes from concurrent at high liquid velocities to countercurrent at low velocities, and CHF values for downflow are lower than for upflow at the same velocity. Additionally, CHF differences between upflow and downflow decrease with increasing inlet velocity because of a gradual diminution of buoyancy effects relative to liquid inertia. Mishima and Nishihara [54] suggested flooding is the cause of CHF for downflow of water at very low velocities. Increasing the velocity from a flooded downflow state caused bubbles to stagnate as the drag force exerted by liquid just balanced buoyancy force. This bubble stagnation produced an even lower CHF than with flooding at lower velocities. By increasing the flow velocity further, bubbles began to flow concurrently downward with the liquid, causing an increase in flow boiling CHF. Gersey and Mudawar [55,56] also demonstrated strong sensitivity of flow boiling CHF of FC-72 to orientation. This sensitivity gradually decreased with increasing flow velocity and increasing subcooling. Like Mishima and Nishihara, they observed vapor flowing opposite to liquid in downflow at very low velocities, stagnating at slightly higher velocities, and moving concurrently with liquid in downflow upon further increases in velocity.

Zhang et al. [57–59] performed extensive studies of the influence of orientation and velocity for flow boiling of FC-72 in a $5.0 \times 2.5$ mm$^2$ rectangular channel heated along one short side. Experiments were performed in different orientations, Fig. 5(a) and (b), including $\theta = 0°$ and 180° corresponding to horizontal flow with the heated wall facing upwards and downwards, respectively, and $\theta = 90°$ and 270° corresponding to vertical upflow and downflow, respectively. Fig. 5(a) shows vapor behavior captured by Zhang et al. [57] at CHF- (conditions just preceding CHF) for near-saturated flow ($\Delta T_{sub,o} = 3$ °C) at $U = 0.1$ m/s. This low velocity greatly reduced liquid drag force compared to buoyancy, causing orientation to have a profound influence on CHF mechanism and magnitude. Shown in Fig. 5(a) are four different CHF regimes: (1) *Pool-Boiling Regime* for $\theta = 0°$, (2) *Wavy Vapor Layer Regime* for $\theta = 90°$, (2) *Stratified Regime* for $\theta = 180°$, and (4) *Vapor Stagnation Regime* for $\theta = 270°$. Notice that, because of the low flow velocity, the first three CHF regimes correspond very closely with the Pool Boiling Regimes observed by Howard and Mudawar [52] and depicted in Fig. 4. In the Pool Boiling Regime ($\theta = 0°$), bubbles coalesce along the heated wall before being detached by buoyancy and driven into the liquid core, with weak tendency to flow with the liquid. The Wavy Vapor Layer Regime ($\theta = 90°$) is associated with bubble coalescence into vapor patches that propagate along the heated wall mimicking a continuous wavy vapor layer, closely resembling the Interfacial Lift-off mechanism for vertical flow boiling CHF illustrated in Fig. 2. The Stratification Regime ($\theta = 180°$) occurs when vapor stratifies above the liquid in the form of a thick, fairly smooth layer that covers nearly the entire heated wall. The Vapor Stagnation Regime ($\theta = 270°$) is the result of buoyancy force just balancing the drag force exerted by liquid on the vapor. Two additional CHF regimes were observed at low flow velocities that are not shown in Fig. 5(a). A *Separated Concurrent Vapor Flow Regime* was encountered at velocities slightly greater than $U = 0.1$ m/s, when liquid drag began to exceed buoyancy. Conversely, a *Vapor Counter Flow Regime* was detected at velocities below 0.1 m/s, where buoyancy exceeded liquid drag, pushing the vapor backwards towards the channel inlet. Aside from these drastic differences in vapor behavior, Fig. 5(a) shows the large differences in CHF magnitude among the four orientations at $U = 0.1$ m/s.

Fig. 5(b) depicts vapor behavior captured by Zhang *et al.* [57] for near-saturated flow ($\Delta T_{sub,o} = 3$ °C) at $U = 1.5$ m/s. This high velocity greatly increases drag forces, dwarfing any buoyancy effects, which is manifest by all four orientations yielding the same Wavy Vapor Layer Regime and fairly equal CHF values. Overall, these findings demonstrate the importance of high flow velocity as a means to overcome body force effects.

Another important parameter that influences CHF is subcooling. High subcooling serves to greatly reduce the size of coalescent vapor masses, thereby decreasing the influence of body force for a given velocity [60,61]. Fig. 6 shows increasing velocity and subcooling increase both CHF magnitude and the sensitivity of CHF to velocity [61].

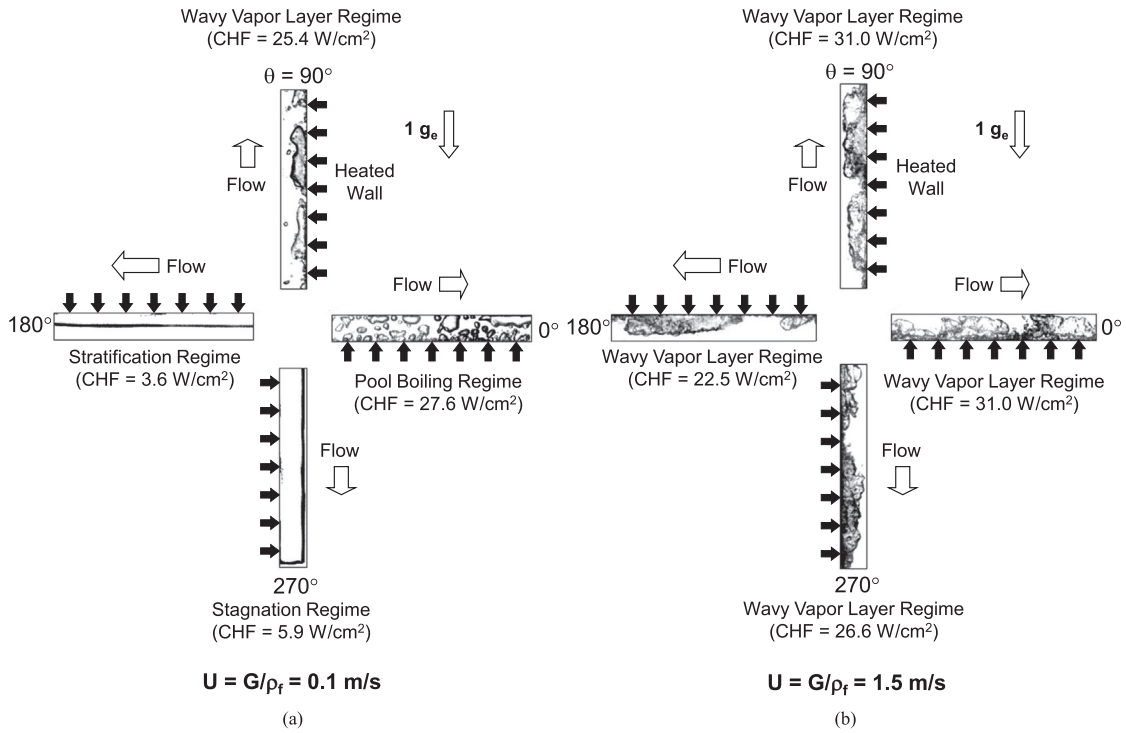


**Fig. 5.** Near saturated ($\Delta T_{sub,o}$ = 3 °C) flow boiling CHF regimes at 1 $g_e$ corresponding to different flow orientations for inlet liquid velocities (a) $U = G/\rho_f$ = 0.1 m/s and (b) $U = G/\rho_f$ = 1.5 m/s. CHF regime and magnitude are highly dependent on orientation for the lower velocity and independent of orientation for the higher velocity [57].

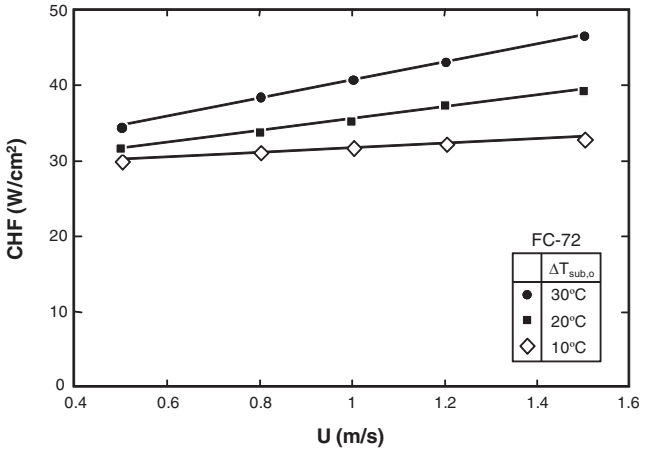


**Fig. 6.** Variation of CHF with mean inlet liquid velocity for three subcoolings [61].

Kharangate et al. and Konishi et al. extended the flow boiling CHF experiments of Zhang et al. to operating conditions where the fluid enters the channel as a saturated two-phase mixture for vertical upflow [39], horizontal flow with the heated wall upward facing [62], and for eight orientations [40,63,64]. They utilized the same experimental apparatus as Zhang et al. excepting the use of a preheater upstream from the flow channel to condition the working fluid, FC-72, to the desired inlet quality $x_{e,in}$. Compared to the flow regimes captured earlier by Zhang et al. for pure liquid inlet conditions, only the *Pool Boiling Regime*, *Stratification Regime* and *Wavy-Vapor Layer Regime* were observed. Kharangate et al. and Konishi et al. hypothesized that the increasing inlet quality increases the velocities of vapor and liquid and the shear force in between, thereby overcoming the influence of body force more effectively than with a pure liquid inlet. Fig. 7(a) shows a polar plot of CHF data measured by Konishi *et al.* [63] for eight orientations and velocities ranging from $G/\rho_f$ = 0.126–1.130 m/s with an inlet quality of $x_{e,in}$ = 0.01. The influence of orientation is quite pronounced for the two lowest velocities of $G/\rho_f$ = 0.126 and 0.224 m/s, especially at $\theta$ = 225°, where CHF values are vanishingly small. There is a diminution of orientation effects starting at the middle velocity of $G/\rho_f$ = 0.398 m/s, and further diminution at the two higher velocities of $G/\rho_f$ = 0.712 and 1.130 m/s. Overall, orientations involving a combination of upflow and/or upward-facing heated wall ($\theta$ = 0°, 45° and 90°) produce higher CHF than downflow and/or downward-facing heated wall ($\theta$ = 180°, 225° and 270°). Fig. 7(b) shows CHF data for velocities ranging from $G/\rho_f$ = 0.126–0.712 m/s at a much larger inlet quality of $x_{e,in}$ = 0.19. Like Fig. 7(a), the influence of orientation for the lowest velocity of $G/\rho_f$ = 0.126 m/s is quite pronounced and yields a vanishingly small CHF value for $\theta$ = 225°. But unlike Fig. 7(a), orientation effects are markedly weaker for $G/\rho_f$ = 0.224 m/s at $x_{e,in}$ = 0.19 compared to $x_{e,in}$ = 0.01. The influence of orientation is further degraded for the two higher velocities of $G/\rho_f$ = 0.398 and 0.712. Comparing Fig. 7(a) and (b) shows that, for equal $G/\rho_f$, increasing inlet quality reduces the sensitivity of CHF to orientation. This reduced sensitivity can be explained by higher velocities of the two phases increasing the magnitude of shear and drag forces compared to buoyancy.

### 2.4. Using tilted flow boiling experiments to derive criteria for negating body force effects

Zhang et al. [65] developed criteria for negating the influence of body force on flow boiling CHF with $x_{e,in} \leqslant 0$. Three separate criteria were proposed: (a) overcoming the influence of the component of gravity perpendicular to the heated wall, (b) overcoming the influence of the component of gravity opposite to the direction of fluid flow, (c) ensuring that the wavelength associated with instability of the liquid–vapor interface is smaller than the heated length to facilitate liquid contact with wall.

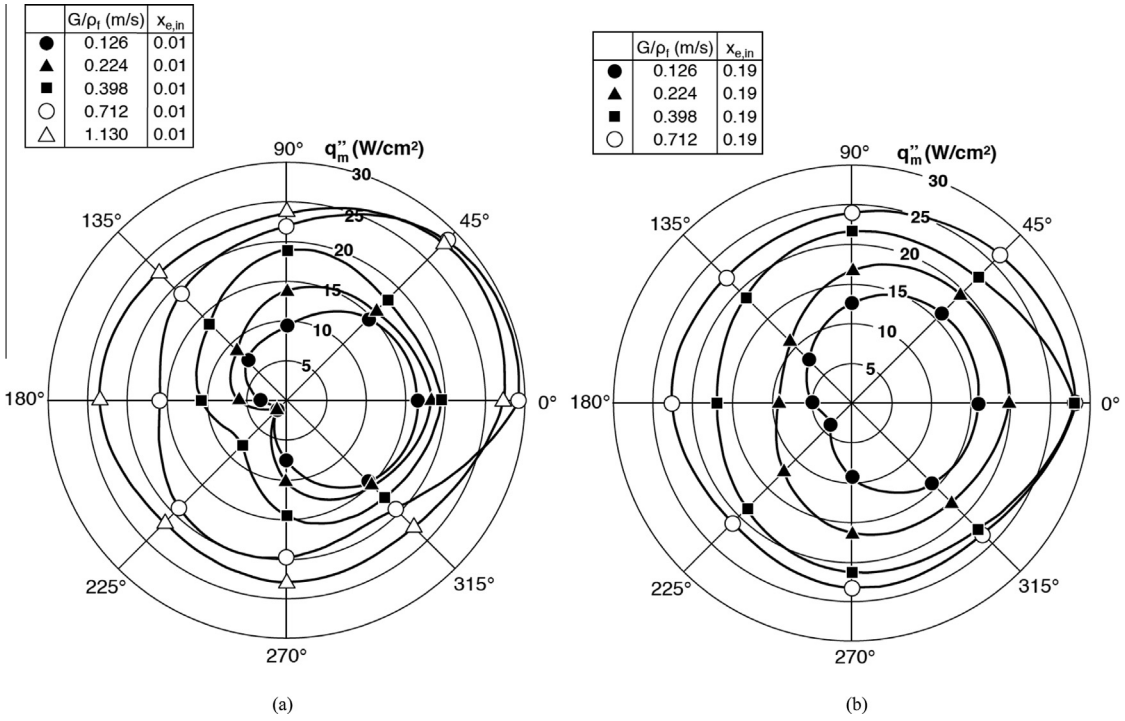


**Fig. 7.** Variation of CHF with flow orientation for different FC-72 mass velocities at (a) $x_{e,in} = 0.01$ and (b) $x_{e,in} = 0.19$ [63].

The criterion for negating the influence of the component of gravity perpendicular to the heated wall is derived as follows. The *Wavy-Vapor Layer Regime* that is dominant for near vertical orientations at low velocities and for all orientations at high velocities can be described with the aid of classical instability theory based on the assumption of a sinusoidal vapor–liquid interface. The critical wavelength, $\lambda_c$, of the interface, which is used to describe the vapor–liquid interface adjacent to the heated wall, is given by

$$\frac{2\pi}{\lambda_c}\frac{\sigma(\rho_f+\rho_g)}{\rho_f\rho_g(U_g-U_f)^2}=\frac{1}{2}\left\{1+\sqrt{1+4\frac{(\rho_f-\rho_g)(\rho_f+\rho_g)^2\sigma g_e\cos\theta}{\rho_f^2\rho_g^2(U_g-U_f)^4}}\right\}. \tag{3}$$

where $U_g$ and $U_f$ are the mean velocities of the vapor and liquid layers, respectively, and $g_e\cos\theta$ the component of gravity perpendicular to the heated wall. Eq. (3) indicates that interfacial instability is governed by the combined influences of inertia, surface tension, and component of gravity perpendicular to the heated wall. Notice that the influence of gravity becomes negligible when

$$\left|\frac{(\rho_f-\rho_g)(\rho_f+\rho_g)^2\sigma g_e\cos\theta}{\rho_f^2\rho_g^2(U_g-U_f)^4}\right|<<\frac{1}{4}, \tag{4}$$

which reduces Eq. (3) to

$$\lambda_c=\frac{2\pi\sigma(\rho_f+\rho_g)}{\rho_f\rho_g(U_g-U_f)^2}, \tag{5}$$

regardless of body force. Eq. (5) can also be presented in terms of the Bond and Weber numbers,

$$\left|\frac{Bo}{We^2}\right|=\left|\frac{(\rho_f-\rho_g)(\rho_f+\rho_g)^2\sigma g_e\cos\theta}{\rho_f^2\rho_g^2(U_g-U_f)^4}\right|<<\frac{1}{4}, \tag{6}$$

where

$$Bo=\frac{(\rho_f-\rho_g)g_e\cos\theta L^2}{\sigma} \tag{7}$$

and

$$We=\frac{\rho_f\rho_g(U_g-U_f)^2L}{(\rho_f+\rho_g)\sigma}. \tag{8}$$

This criterion was examined by substituting the phase velocity by the characteristic velocity of the flow channel, $U$, and the component of gravity perpendicular to the heated wall by the maximum value of the same component, $g$. Since the CHF data of Zhang et al. showed little dependence on orientation for $U \sim 1.5$ m/s, the magnitude of $Bo/We^2$ corresponding to $U = 1.5$ m/s was used as a criterion for overcoming body force effects on CHF, which, for any gravity field, $g$, can be simplified to

$$\frac{Bo}{We^2}=\frac{(\rho_f-\rho_g)(\rho_f+\rho_g)^2\sigma g}{\rho_f^2\rho_g^2U^4}\leqslant 0.09. \tag{9}$$

The criterion for negating the influence of gravity parallel to the heated wall and opposite the direction of fluid flow uses an expression for rise velocity of a large coalescent slug flow bubble relative to liquid [66],

$$U_\infty=0.35\frac{\left[(\rho_f-\rho_g)g_e|\sin\theta|D_h\right]^{1/2}}{\rho_f^{1/2}}, \tag{10}$$

where $D_h$ is the hydraulic diameter of the channel. When $U_\infty$ exceeds the liquid velocity, the vapor tends to flow backwards relative to the liquid inducing flooding, and when the two velocities are equal the vapor stagnates along the channel. A sufficient criterion for preventing flooding is $U_\infty \ll U$, which, for $\sin\theta = 1$ (corresponding to strongest orientation influence), can be presented in terms of the Froude number,

$$\left|\frac{1}{Fr}\right|=\left|\frac{(\rho_f-\rho_g)\sigma g_eD_h}{\rho_fU^2}\right|\leqslant 8.16. \tag{11}$$

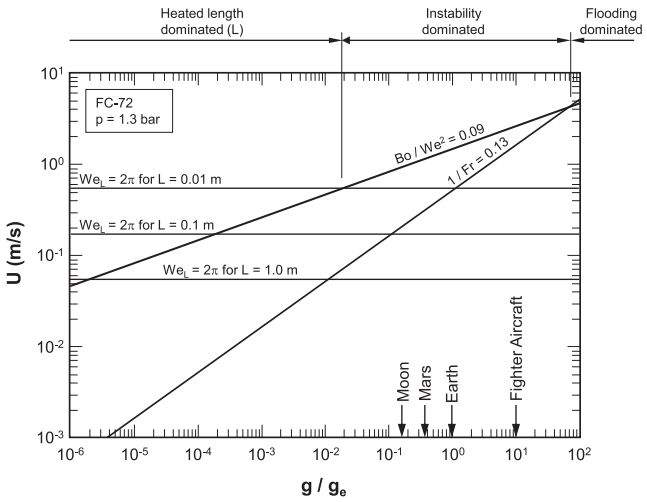


**Fig. 8.** Determination of minimum flow velocity required to satisfy all criteria for negating gravity effects on flow boiling CHF [65].

Since the CHF data of Zhang et al. showed flooding is avoided for $U \geqslant 0.5$ m/s, the criterion for precluding the occurrence of this anomaly in any gravity, $g$, can be reduced to

$$\frac{1}{Fr} = \frac{(\rho_f - \rho_g) g D_h}{\rho_f U^2} \leqslant 0.13. \tag{12}$$

To enable liquid contact with the heated wall, it is crucial that the interfacial wavelength be smaller than the heated length, i.e., $\lambda_c \leqslant L$. This comprises the third criterion for negating the influence of body force. Using the expression for $\lambda_c$ from Eq. (5), this criterion can be expressed as a Weber number criterion,

$$We = \frac{\rho_f \rho_g (U_g - U_f)^2 L}{(\rho_f + \rho_g)\sigma} \geqslant 2\pi. \tag{13}$$

Fig. 8 shows the minimum velocity required to satisfy the above three criteria as a function of $g/g_e$, the ratio of prevailing gravity to Earth gravity. Avoiding all body force effects requires that flow velocity exceed values predicted by each of the three criteria; only one of these criteria is dominant for a given value of $g/g_e$. Fig. 8 shows fairly appreciable flow velocities are required to overcome flooding, should a large gravitational field of $g/g_e > 75$ be present in a direction opposite to the liquid flow. Instability effects are dominant for $g/g_e < 75$ in a direction perpendicular to the heated wall; this is where surface tension effects become increasingly important. Notice that this instability criterion spans Earth, Lunar and Martian environments. The heater length criterion is dominant for very low values of $g/g_e$. The $g/g_e$ value associated with transition between the instability-dominated and heater-length-dominated regimes is a function of the heated length, with shorter heaters requiring higher velocities to decrease critical wavelength below the heated length. In general, the heater-length-dominated regime is more significant for microgravity conditions.

Recall that the criteria developed by Zhang et al. are based on their own data for which $x_{e,in} \leqslant 0$. Recently, Konishi et al. [64] extended these criteria to two-phase inlet conditions, $x_{e,in} \geqslant 0$. Here, flow velocities increase with increasing $x_{e,in}$. Therefore, stronger inertial effects serve to combat gravity more effectively and satisfy the criteria for negating gravity effects at lower inlet velocities than for $x_{e,in} \leqslant 0$.

### 2.5. Advantages of micro-channels in helping negate body force effects

Decreasing hydraulic diameter of the flow channel increases flow velocity for a given flow rate. This is a key feature of two-phase flow in micro-channels, which provide important advantages to space systems by greatly increasing flow inertia for a given flow rate to help resist body forces effects. These advantages were recently examined by Lee et al. [67,68] who explored flow boiling of FC-72 in a test module containing 80 of 231-μm wide × 1000-μm deep micro-channels in three flow orientations: horizontal, vertical upflow and vertical downflow. Their data showed gravity effects are negated altogether at velocities far smaller than those for macro-channels.

## 3. Pool boiling in reduced gravity

Before reviewing reduced gravity flow boiling, it is useful to examine findings from reduced gravity pool boiling studies concerning such fundamental processes as bubble nucleation, growth and coalescence on a heated wall in the absence of gravity, and the impact of these processes on both nucleate boiling heat transfer and CHF. Table 1 summarizes prior reduced gravity pool boiling studies.

Oka and coworkers performed microgravity pool boiling experiments with *n*-Pentane, R-113 and water in parabolic flight [70], and R-113 and water in a drop shaft [71]. In both types of tests, the fluid's surface tension and latent heat of vaporization had a profound influence on bubble nucleation, growth and coalescence, and on heat transfer effectiveness. Tests with *n*-Pentane and R-113, which possess relatively low surface tension and low heat of vaporization, showed bubbles rarely detach from the heater surface at moderate subcoolings. At low heat fluxes, isolated bubbles slid slowly across the heater surface, constantly coalescing with neighboring bubbles. This sliding motion facilitated liquid replenishment to dryout regions of the surface originally inhabited by the bubbles. At high heat fluxes and/or near-saturated conditions, isolated bubbles grew larger and coalesced with other sliding bubbles with greater frequently, culminating in the formation of a single large bubble that encompassed the majority of the heater surface. Dryout beneath the large bubble ensued, resulting in unsteady rise in the surface temperature. As shown in Fig. 9(a), nucleate boiling is far less effective and CHF significantly smaller for R-113 in microgravity was than in Earth gravity. In microgravity tests with water, whose surface tension and heat of vaporization are significantly greater than those of *n*-Pentane and R-113, Oka et al. observed isolated bubbles detaching from the heater surface almost immediately upon generation, and growing to significantly larger size compared to terrestrial tests. At moderate subcooling, the detached bubbles immediately collapsed into the bulk liquid due to increased condensation. When detached bubbles were propelled into the bulk liquid at saturated or nearly saturated conditions, they remained within the vicinity of the heater surface, constantly coalescing with each other to form a single large vapor bubble, which continued to grow in size by engulfing newly formed bubbles. The high latent heat of vaporization of water delayed the complete evaporation of the thin liquid film beneath the large bubble, evidenced by absence of wall temperature excursions, especially for near-saturated conditions. Continued liquid supply to the thin film at the bubble contact area was confirmed by generation of a secondary bubble within the large bubble, a phenomenon later confirmed for microgravity pool boiling of water by Abe and Iwasaki [78].

Some investigators postulated that thermocapillary or Marangoni convection, typically masked by dominant buoyancy-driven convection in terrestrial conditions, plays a significant role in bubble nucleation and growth in microgravity, and therefore influences heat transfer effectiveness. These convection effects are the result of fluid motion along the vapor–liquid interface and away from the heater surface, induced by surface tension gradients.

**Table 1**
Summary of prior reduced gravity pool boiling studies.

| Author(s) | Microgravity platform | Test fluid | Heater geometry | Test conditions | Remarks |
|---|---|---|---|---|---|
| Abe and Iwasaki (1993) [69] | Sounding rocket (TR-1A) ($2 \times 10^{-4}$ $g_e$, ~ 6 min) | *n*-pentane | BK-7 glass $A_h = 30 \times 30$ mm$^2$ 5 artificial cavities (100 μm diameter) | $p$ = 100, 160 kPa<br>$\Delta T_{sub}$ = 11.1, 25.7 K<br>$q''$ = 5–50 kW/m$^2$ | – Minimal isolated bubble departure promotes coalescence into a large bubble encompassing majority of heater surface<br>– Nucleate heat transfer is degraded in $\mu g_e$ |
| Oka et al. (1995) [70] | Parabolic flight (Caravelle 234) ($10^{-2}$ $g_e$) | *n*-Pentane, R-113, water | BK-7 glass-/indium tin oxide (ITO) transparent coated heater $A_h = 50 \times 50$ mm$^2$ | $p$ = 81-183 kPa<br>$\Delta T_{sub}$ = 2–17 K<br>$T_b$ = 29.2–94.5 °C<br>$q''$ = 30–119 kW/m$^2$ | – Bubbles generated in water are spherical in shape, allowing minimal contact, or are expelled from heater surface; bubbles in other fluids are attached to heater surface over a large contact area<br>– Boiling heat transfer is deteriorated for water over entire nucleate boiling regime, but for other fluids only at high heat fluxes<br>– CHF for organic fluids is degraded by 40% in $\mu g_e$ compared to terrestrial data |
| Oka et al. (1996) [71] | Drop shaft (JAMIC) ($10^{-5}$ $g_e$, ~10 s) | R-113, water | Aluminum plate/stainless steel foil coating $A_h$ = 40, 80 mm square and Pryex/ITO coated $A_h$ = 30 mm square | $\Delta T_{sub}$ = 6–22 K<br>$q''$ < 64 kW/m$^2$ | – For water, capillarity-driven bubble detachment sustains nucleate boiling over a range of heat flux up to CHF<br>– Periodic bubble formation in R-113 occurs on relatively small fraction of heater surface, excluding discrete areas encompassed by larger vapor masses<br>– CHF is degraded by 20–30%<br>– CHF dependence on liquid subcooling is stronger in $\mu g_e$ than in terrestrial conditions |
| Lee and Merte (1996) [72] | NASA Space Shuttle (STS-47, 57, 60) ($10^{-4}$ $g_e$) | R-113 | Quartz/semi-transparent gold film $A_h = 19.05 \times 38.1$ mm$^2$ | $p$ = 107.7–117.3 kPa<br>$\Delta T_{sub}$ = 0.7–3.2 K<br>$T_b$ = 48.6 °C<br>$q''$ = 1.8-6.5 W/cm$^2$ | – Hemispherical models developed to globally describe bubble growth in $\mu g_e$ and determine upper and lower bounds of the growth |
| Ohta et al. (1997) [73] | Parabolic flight (MU-300) ($10^{-2}$ $g_e$, 2 $g_e$) | Water/ ethanol | Sapphire glass/ITO coated $D_h$ = 50 mm | $p$ = 100, 20 kPa<br>$\Delta T_{sub}$ = 3–11 K<br>$q''$ = 30–290 kW/m$^2$ | – At low heat fluxes, nucleate boiling heat transfer coefficient in $\mu g_e$ is larger than in 2 $g_e$, but no differences are observed at high fluxes<br>– Enhancement or deterioration of local heat transfer dictated by microlayer formation beneath primary bubbles just after their formation |
| Straub et al. (1997), Straub (2000, 2002) [74–76] | Spacelab (Mission IML-2, STS-65) ($10^{-4}$ $g_e$) | R-11 | Thermistor $D_h$ = 0.26 mm | $p$ = 650 kPa<br>$T_b$ = 30–70 °C<br>$T_w$ = 150–200 °C<br>$q'' \leqslant$ 900 kW/m$^2$ | – There is no observable influence of gravity on heat transfer in nucleate boiling regime<br>– With moderate subcooling, heat transfer coefficient in film boiling and transition boiling is degraded by 50% in $\mu g_e$ compared to terrestrial conditions<br>– With moderate subcooling, a thermocapillary jet is formed in the film boiling regime on a primary vapor bubble, which effectively transports high heat fluxes into the bulk liquid |
| Ohta et al. (1999) [77] | Sounding rocket (TR-1A) | Ethanol | Sapphire glass/ITO coated $D_h$ = 50 mm | $p$ = 11, 20 kPa<br>$\Delta T_{sub}$ = 3–11 K<br>$T_b$ = 27 °C<br>$q''$ = 30 kW/m$^2$ | – Steady-state nucleate boiling is attainable in $\mu g_e$ except for high heat fluxes or very low liquid subcooling<br>– At high heat fluxes or low liquid subcooling, a large coalescent vapor bubble is formed which lifts off the heater surface because of generation of bubbles at the base; this is speculated to be the dominant mechanism for nucleate boiling heat transfer |
| Abe and Iwasaki (1999) [78] | Drop shaft (JAMIC) ($10^{-5}$ $g_e$, ~10 s) | R-113, R-122/R-12, water/ ethanol | TEMPAX glass/ITO coated $A_h = 20 \times 30$ mm$^2$ | $\Delta T_{sub}$ = 3-18 K | – The Marangoni effect is more pronounced with increased liquid subcooling<br>– Interferograms captured during the bubble evolution suggest the Marangoni effect is governed by temperature gradients in the early stages of bubble growth and later by concentration gradients |
| Kim et al. (2002), Henry and Kim (2004) [79,80] | Parabolic flight (KC-135) (0.01 $g_e$, 1.7 $g_e$) | FC-72 | Platinum resistance heater $A_h$ = 0.65–7.29 mm$^2$ | $\Delta T_{sub}$ = 23.1–31.2 K<br>$T_b$ = 35–54.8 °C<br>$q''$ ~ 0–30 W/cm$^2$ | – In low gravity, CHF increases with increasing subcooling if the dry area beneath the primary bubble is smaller than the heater surface area<br>– Thermocapillary convection at higher superheats and subcooling decreases the size of the primary bubble<br>– In high gravity, bubble departure frequency decreases for the smallest heater array, but is significantly smaller compared to low gravity conditions<br>– For the larger heaters, increased subcooling decreases departure frequency of the primary bubble, but the time and surface averaged heat transfer is unaffected |
| Merte (2004, 2006) [81,82] | NASA Space Shuttle (STS-47, 57, 60, 72, 77) ($10^{-4}$ $g_e$) | R-113 | Quartz/semi-transparent gold film $A_h = 19.05 \times 38.1$ mm$^2$ | $\Delta T_{sub}$ = 0.3–22.2 K<br>$q''$ = 0.5–8 W/cm$^2$ | – High subcooling produces small vapor bubbles within the vicinity of heater surface; these bubbles are driven along the surface by thermocapillary effects<br>– Computations show momentum transfer of the small nucleating bubbles bombarding the primary vapor bubble are countered only by the thermocapillary force on the primary bubble |

(*continued on next page*)

**Table 1** (*continued*)

| Author(s) | Microgravity platform | Test fluid | Heater geometry | Test conditions | Remarks |
|---|---|---|---|---|---|
| Sodtke et al. (2006) [83] | Parabolic flight (ESA A-300) | FC-72 | Aluminum plate/stainless steel foil (10 μm) $A_h$ = 11.76 cm$^2$ | $\Delta T_{sub}$ = 3–5 K<br>$q$ = 12–15 W | – High resolution wall temperature distribution close to the thin liquid film near the base of the vapor bubble in nucleate boiling is captured using unencapsulated thermochromic liquid crystals<br>– A strong wall temperature drop occurs close to the thin liquid film where the liquid–vapor interface approaches the heater surface |
| Zhao et al. (2007, 2008) [84,85] | 22nd Chinese recoverable satellite ($10^{-3}$–$10^{-5}$ $g_e$) | R-113 | Platinum wire 60 μm diameter, 30 mm long | $p$ = 101 kPa<br>$\Delta T_{sub}$ = 26.2 K<br>$T_b$ = 21.3 °C | – The two-phase heat transfer coefficient is enhanced in $\mu g_e$<br>– Lateral bubble oscillation along the wire leads to bubble coalescence and causes bubble departure<br>– A thorough dynamic analysis of departure criteria is performed for bubbles growing in $\mu g_e$ |
| Zhao et al. (2009) [86] | Chinese recoverable satellite (SJ-8) ($10^{-3}$–$10^{-5}$ $g_e$) | FC-72 | $AL_2O_3$ ceramic $A_h$ = 15 × 15 mm$^2$ | $p$ = 57.2–111.7 kPa<br>$\Delta T_{sub}$ = 18.4–36.9 K<br>$T_b$ = 16.7–43.3 °C<br>$\Delta T_{sat}$ = 11–76 K | – Both the two-phase heat transfer coefficient and CHF increase with increases in subcooling or pressure<br>– CHF is degraded by about a third in $\mu g_e$ compared to terrestrial conditions |
| Raj et al. (2009) [87] | Parabolic flight (ESA Airbus A300) (0.01 $g_e$, 1.8 $g_e$) | nPFH | Platinum resistance heater $A_h$ = 12.25–49.0 mm$^2$ | $p$ = 1 atm<br>$\Delta T_{sub}$ = 26 °C<br>$T_w$ = 65–100 °C | – Drastic variations of heat flux between low and high gravity preclude the possibility of deriving a unified power law dependence across all gravity levels<br>– High dissolved gas concentrations cause nucleate boiling heat transfer to be enhanced in high gravity and degraded in low gravity<br>– Nucleation site density remains fairly constant under gravity levels that foster capillary lengths significantly smaller than the characteristic length of the heater |
| Kannengieser et al. (2010) [88] | Sounding rocket (Maser 11) ($5 \times 10^{-4}$ $g_e$, ~6.5 min) | HFE-7000 | Copper $A_h$ = 1 cm$^2$ | $p$ = 120–330 kPa<br>$T_b$ = 25 °C<br>$q$ = 0-5 W | – Boiling is dominated by formation of a large primary bubble due to coalescence of smaller bubbles on the heater surface, driven by Marangoni convection<br>– For $T_w < T_{sat}$, bubble growth is impeded because of weak evaporation, and heat transfer is governed mainly by Marangoni convection<br>– For $T_w > T_{sat}$, significant bubble growth is intensified by enhanced bubble nucleation at the wall, and heat transfer is governed mainly by evaporation |
| Xue et al. (2011) [89] | Drop tower (Beijing NMLC) ($10^{-2}$ $g_e$, ~3.6 s) | FC-72 | Silicon chip $A_h$ = 10 × 10 mm$^2$ | $p$ = 102 kPa<br>$\Delta T_{sub}$ = 41 K<br>$T_b$ = 14.6 °C<br>$q''$ = 3.38–11.59 W/cm$^2$ | – At low heat fluxes, there is minimum coalescence amongst nucleating bubbles, which maintain contact with the heater surface because of strong thermocapillary convection around the bubbles<br>– Upon increasing heat flux, bubble size and frequency increase<br>– At high heat fluxes, a large coalescent bubble rapidly forms and completely covers the heater surface, leading to local dryout at the bubble base and deterioration of nucleate boiling heat transfer |
| Raj et al. (2012) [90] | International Space Station (ISS) ($10^{-6}$ $g_e$) | nPFH | Platinum resistance heater $A_h$ = 17.6–49.0 mm$^2$ | $p$ = 0.58–1.86 atm<br>$\Delta T_{sub}$ = 1–26 °C<br>$T_w$ = 55–107.5 °C | – A gravity scaling parameter for $\mu g_e$ pool boiling heat flux developed earlier by the same authors is modified and shows excellent agreement with experimental results |
| Dhir et al. (2012) [91] | International Space Station (ISS) ($1.2 \times 10^{-7}$–$6 \times 10^{-7}$ $g_e$) | nPFH | Aluminum $D_h$ = 89.5 mm 5 artificial cavities (10 μm diameter) | $p$ = 51–243 kPa<br>$T_b$ = 30–59 °C<br>$T_w$ = 40–80 °C | – Low wall superheat promotes lateral coalescence of bubbles into a single coalescent bubble that grows progressively on the heater surface |
| Souza et al. (2013) [92] | Sounding rocket (Brazil VSB 30) ($10^{-6}$ $g_e$, ~6.5 min) | *n*-Pentane | Copper disks $D_h$ = 12 mm | $p$ = 117–132 kPa<br>$\Delta T_{sub}$ = 14.3–15.8 K<br>$T_b$ = 25.6–28.3 °C<br>$q \leqslant 60$ kW/m$^2$ | – Subcooled nucleate boiling behavior is investigated for different bulk temperatures and gap sizes<br>– For the smallest gap size, the two-phase heat transfer coefficient is degraded by about 20% in $\mu g_e$ compared to terrestrial conditions<br>– For the largest gap size, the two-phase heat transfer coefficient decreases with increasing heat flux |

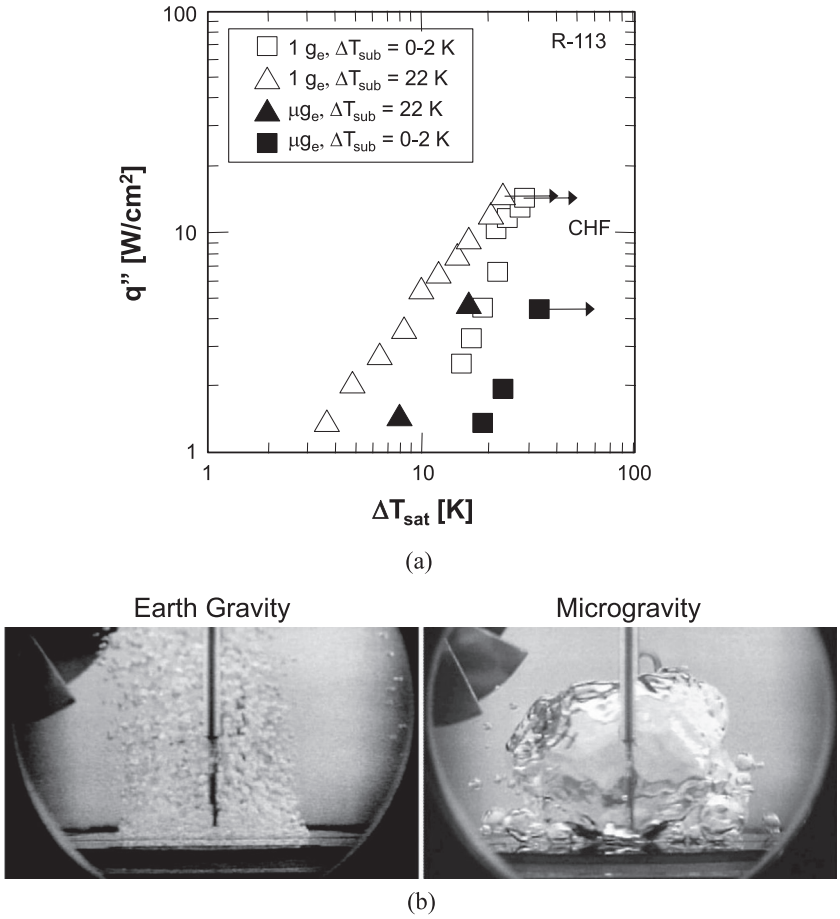


**Fig. 9.** (a) Pool boiling curves for R-113 in microgravity and Earth gravity at two levels of subcooling (adapted from Oka et al. [71]). (b) Photos of pool boiling of R-113 in Earth gravity and microgravity (courtesy NASA).

Predominantly observed in subcooled boiling, these convection effects resulted in jet streams around the nucleating bubbles, which assisted the transport of heat from the bubbles to the bulk liquid. These effects were identified by Straub [75] in long-duration microgravity pool boiling experiments with R-11 on a hemispherical heater that were performed in Spacelab mission IML-2. Straub [76] later performed a thorough heat transfer analysis of the contributions of thermocapillary convection in microgravity. Overall, the strength of the thermocapillary jet, which was measured by particle image velocimetry (PIV), increased with increasing heat flux. However, this behavior was highly influenced by the degree of subcooling. In saturated conditions, they measured zero jet velocity. Upon slightly increasing the subcooling, the jet velocity increased rapidly to a maximum level, but decreased back to zero at high subcooling. In subcooled boiling, they postulated bubble growth is dictated by a balance between evaporation at the bubble base and condensation at the bubble cap. Differences between the two rates resulted in temperature gradients that induced vapor flow within the bubble. Straub proposed that thermocapillary convection observed in subcooled conditions is induced by accumulation of minute amounts of inert gases that are driven by the internal bubble vapor flow towards the condensation region.

Merte and co-workers [81,82] also conducted long-duration microgravity pool boiling experiments with R-113 onboard NASA's Space Shuttle (STS-47, 57, 60, 72, 77). They used a flat $19.05 \times 38.1$ mm$^2$ rectangular heater consisting of a semi-transparent gold film deposited on a quartz substrate. Their experiments covered subcoolings of $\Delta T_{sub} = 0.3$–$22.2$ K and heat fluxes of $q'' = 0.5$–$8$ W/cm$^2$. For moderate subcoolings and low heat fluxes, a large vapor bubble formed and hovered in the vicinity of the heater surface while smaller bubbles nucleated underneath. For low heat fluxes, they postulated that the thermocapillary reaction force that would otherwise push the large vapor bubble towards the heater surface and cause dryout is opposed by momentum of small bubbles coalescing into the large bubble. This helps maintain liquid replenishment of the heater surface, permitting steady nucleate boiling and even yielding heat transfer coefficients at low heat fluxes that are greater than those realized in terrestrial conditions. Excepting their highest subcooling condition, all tests conducted at the highest heat flux culminated in partial or complete dryout as a large vapor bubble engulfed the entire heater surface leading to unsteady rise in the surface temperature and appreciable reduction in the heat transfer coefficient. Fig. 9(b) shows photos of bubble formation in microgravity obtained in Space Shuttle experiments compared to those in Earth gravity. Notice how a single large bubble is formed in microgravity engulfing the entire heater surface without a tendency to depart from the surface. On the other hand, many smaller discrete bubbles are formed in Earth gravity, which are pulled away from the surface by buoyancy.

A common observation in the above and other microgravity pool boiling experiments is formation of an unusually large bubble, which often engulfs the entire heater surface, a phenomenon rarely encountered in terrestrial conditions. This phenomenon can be explained by the Capillary or Laplace length, which dictates the size of a bubble in response to surface tension and gravity. In

microgravity, Capillary length is unusually large, which explains the formation of the unusually large bubble. Another important consideration is how the Capillary length compares to heater size.

Kim and co-workers conducted microgravity pool boiling experiments with FC-72 in several parabolic flight campaigns, and recently with nPFH onboard the ISS, and addressed the influence of Capillary length. They obtained impressive high-speed video images of pool boiling in both microgravity and high gravity (1.7 $g_e$) onboard NASA's KC-135 jet [79,80]. They developed a unique heater surface consisting of several arrays of platinum resistance heaters that were controlled by a bank of feedback circuitry to achieve constant surface temperature. Subcooled pool boiling of FC-72 was achieved using three heater sizes, 0.65, 2.62 and 7.29 $mm^2$. In microgravity, absence of buoyancy allowed surface tension to play a dominant role, culminating in the formation of a single large bubble regardless of heater size. On the other hand, tests at 1.7 $g_e$ showed a dependence on heater size, with the smallest heater yielding a single primary bubble due to proximity of this heater's size to the Capillary length, while the largest heater was able to accommodate multiple nucleation sites and generate a primary bubble with neighboring satellite bubbles. Kim's team later performed long-duration microgravity tests onboard the ISS utilizing the Boiling eXperiment Facility (BXF) [90], which incorporated two experiments within a single apparatus: Kim and co-workers' Microheater Array Boiling Experiment (MABE), and the Nucleate Pool Boiling Experiment of Dhir et al. [91]. Experimental results from MABE led to the following important findings concerning pool boiling in microgravity: (1) the onset of nucleate boiling (ONB) in microgravity occurs at lower surface superheat compared to terrestrial data, (2) increasing system pressure decreases the superheat required for ONB, which enhances heat transfer throughout the nucleate boiling regime up to CHF, (3) heat transfer is enhanced with increased subcooling and degraded with decreased subcooling, where a large bubble engulfs the entire heater surface, (4) the boiling curve for high gravity is heater size dependent, and (5) with decreasing heater size, heat transfer is enhanced at high subcooling and degraded at low subcooling.

Dhir and co-workers [91] conducted long-term nucleate boiling experiments onboard the ISS. Testing was performed with nPFH on an aluminum wafer equipped with an array of strain gage heaters and thermistors, and featuring five 10-μm diameter artificial cavities. They compared single and multiple bubble dynamics and heat transfer data with predictions of numerical simulation tools developed earlier by Son et al. [93]. The numerical model accounts for interfacial condensation at the bubble cap as well as dissolved gasses present in the liquid. Numerical single-bubble nucleation results predicted the experimental transient bubble shape and size remarkably well. Like previous investigators, Dhir and co-workers observed the formation of single large primary bubble from coalescence of lateral bubbles merging on the heater surface. At high superheats, the large bubble was able to lift off the heater surface and hover within close proximity of the surface, continuously growing in size by pulling in additional bubbles generated on the surface.

Despite the important fundamental knowledge gained from microgravity pool boiling experiments, two overriding concerns point to serious challenges in implementing pool boiling in space applications: (i) formation of an unusually large bubble that engulfs the entire heater surface, and (ii) appreciable reduction in CHF compared to terrestrial data. These concerns point to the need for another force to overcome these effects. By relying on fluid inertia to dwarf other forces, flow boiling systems provide an effective means for controlling bubble growth and maintaining liquid replenishment of the heater surface to boast CHF.

## 4. Two-phase flow and heat transfer in reduced gravity

### 4.1. Types of two-phase flow and heat transfer microgravity studies and prior review articles

Three different types of studies have been undertaken to assess the influence of microgravity on two-phase flow and heat transfer: (1) adiabatic experiments aimed at identifying dominant two-phase flow patterns and measuring two-phase pressure drop, (2) steady-state heat transfer experiments that explore bubble nucleation and growth, and measure nucleate boiling heat transfer and CHF, and (3) quenching experiments that measure the same parameters but in transient experiments.

Several articles have recently been published to review the limited literature concerning these studies. They include an early article by Antar [94] on two-phase flow dynamics, followed by a series of reviews on two-phase heat transfer [95–98]. More recently, Di Marco [99] reviewed the mechanisms governing both pool boiling and flow boiling in microgravity, with added focus on the influence of electrical field on boiling. Ohta and Baba [100] highlighted their microgravity boiling research and discussed an experimental facility to be launched in a few years to the ISS to conduct long-duration flow boiling experiments. Baldassari and Marengo [101] summarized findings from both terrestrial and microgravity flow boiling literature, with particular focus on the influence of the Eötvös number for flow boiling in terrestrial small-channel experiments and in low gravity.

### 4.2. Adiabatic two-phase flow studies

Since the early adiabatic two-phase microgravity experiments of Hepner et al. [102], researchers quickly realized the vast differences in interfacial behavior between terrestrial and reduced gravity environments. Only three of the classical flow patterns in tubes are commonly achieved in reduced gravity: bubbly, slug and annular flows, with a fourth frothy slug–annular flow pattern observed in a few studies, as depicted in Fig. 10(a), based on combinations of superficial velocities of vapor and liquid, $j_g$ and $j_f$, respectively [103]. Choi et al. [104] compared air–water flow patterns along a 10-mm diameter tube in microgravity ($\mu g_e$) and hypergravity (2 $g_e$) aboard an MU-300 aircraft, and in terrestrial gravity (1 $g_e$). Their findings point to the important role of flow velocities in influencing, not only flow pattern, but also the relative importance of body force. As shown in Fig. 10(b), low flow velocities allow surface tension forces to play a dominant role in $\mu g_e$, yielding bubbly flow, whereas 1 $g_e$ and 2 $g_e$ environments produce stratified and plug flows, respectively, for the same velocities. On the other hand, high velocities cause flow inertia to dwarf any surface tension or gravity effects, yielding similar flow patterns for all gravity levels.

Dukler et al. [105] performed adiabatic air–water two-phase flow experiments in a 9.52-mm diameter and 0.475-m long horizontal tube in the NASA Lewis 100-ft drop tower and in parabolic flight onboard the NASA Lewis Learjet. Three classical flow patterns were observed: bubbly, slug and annular flow. Transition from bubbly to slug flow was based on bubble size and concentration in bubbly flow that promotes coalescence, which was estimated to occur at $\alpha = 0.45$. In the absence of drift between the phases in microgravity bubbly flow, the mean velocities of vapor and liquid are equal. Using $\alpha = 0.45$, this yields the following relation for transition from bubbly to slug flow.

$$j_f = j_g\left(\frac{1-\langle\alpha\rangle}{\langle\alpha\rangle}\right) = 1.22j_g, \tag{14}$$

where $\langle\alpha\rangle$ is the void fraction averaged over the cross-sectional area of the tube. For transition from slug to annular flow, they postulated

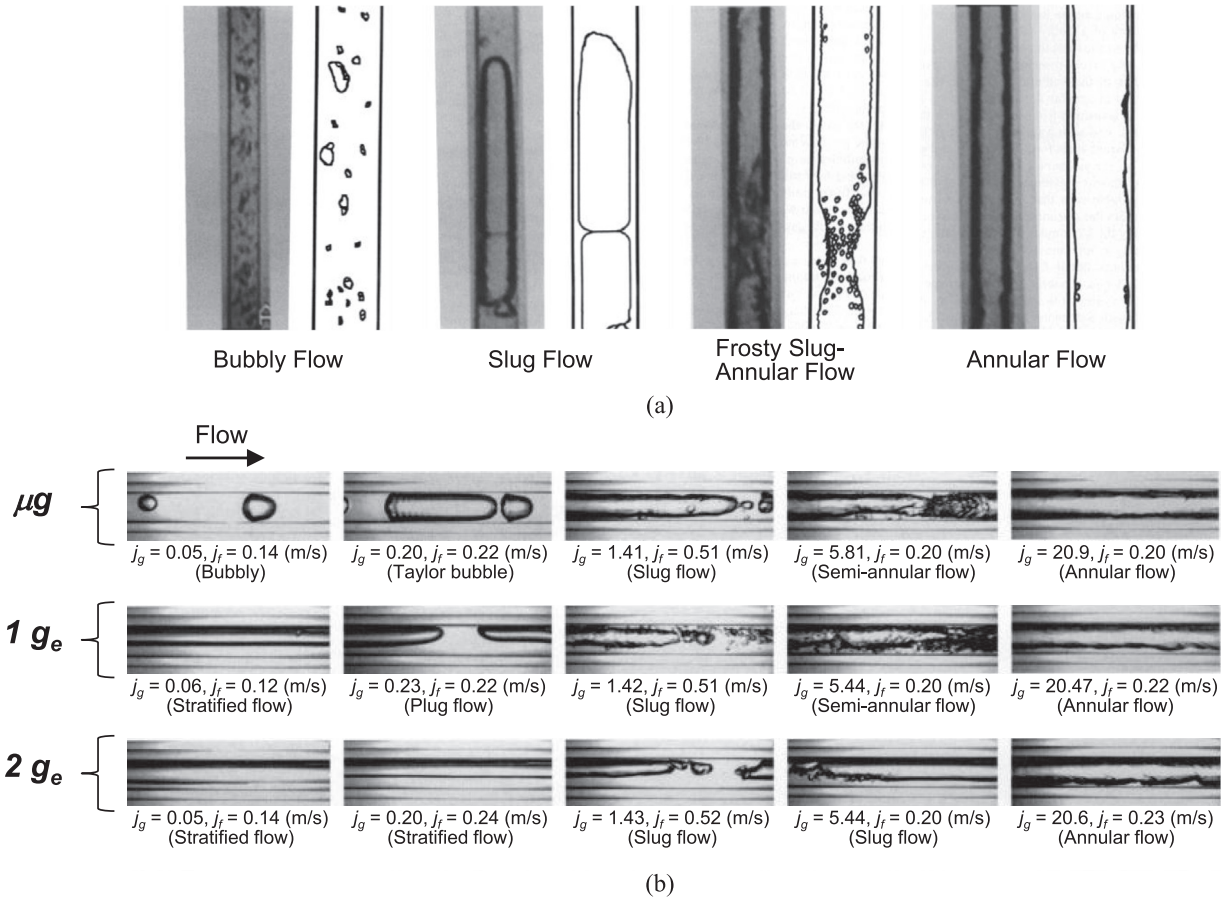


**Fig. 10.** (a) Air–water two-phase flow patterns in microgravity (adapted from Zhao and Rezkallah [103]). (b) Air–water flow patters along a 10-mm diameter tube in microgravity ($\mu g_e$), terrestrial gravity (1 $g_e$), and hypergravity (2 $g_e$) (adapted from Choi et al. [104]).

that increased gas flow rate promotes elongation of Taylor bubbles in the axial direction. As the liquid slugs separating these bubbles become relatively short, variations in the local velocity or adjacent film thickness cause the slugs to rupture, allowing surface tension forces to draw the liquid towards the wall and establish the characteristic annular flow. The slug–annular transition was obtained by equating the following Drift-Flux relations for slug and annular flow, respectively.

$$\frac{j_g}{j_f + j_g} = C_0\langle\alpha\rangle, \tag{15a}$$

and

$$\frac{\langle\alpha\rangle^{5/2}}{(1-\langle\alpha\rangle)^2} = \left(\frac{f_i}{f_w}\right)\left(\frac{\rho_g}{\rho_f}\right)\left(\frac{j_g}{j_f}\right)^2, \tag{15b}$$

where $C_o$ is the distribution parameter in the Drift Flux model. The interfacial friction factor, $f_i$, in Eq. (15b) is determined from the empirical correlation [66]

$$\frac{f_i}{f_g} = 1 + 150(1-\alpha^{1/2}), \tag{16}$$

and the wall friction factor, $f_w$, and gas layer friction factor, $f_g$, using the Blasius relation with a Drift Flux distribution parameter of $C_o = 1.25$.

Bousman et al. [106–108] continued the work of Dukler et al. by conducting parabolic flight adiabatic tests using two horizontal tubes: a smaller tube ($D = 12.7$ mm) in NASA's Learjet Model 25, and larger tube ($D = 25.4$ mm) in NASA's KC-135 jet. In addition to investigating the influence of tube diameter, they explored surface tension effects by testing three different fluid combinations: air–water, air- 50–50 wt% water/glycerin, and air–water/Zonyl FSP. Observations of interfacial behavior proved turbulent oscillations are more pronounced in the larger tube, which enhanced bubble coalescence, causing a significant shift in void fraction corresponding to bubbly–slug transition; this shift was less pronounced for the reduced surface tension liquids (glycerin, Zonyl FSP). Therefore, different relations were recommended for bubbly–slug transition based on different fluid combinations. For both tubes, they estimated slug–annular transition to occur at $\alpha = 0.75$ for air–water and air–water/Zonyl FSP, and $\alpha = 0.70$ for air–water/glycerin. They used the same general methodology proposed by Dukler et al. to derive an alternative Drift-Flux relation for slug–annular transition.

Colin and coworkers [109–114] performed several adiabatic air–water two-phase flow experiments in microgravity. Colin et al. [109] compared flow patterns in a 40-mm, 3.14-m long tube in parabolic flight with those in vertical upflow at 1 $g_e$. Comparing results with those of Dukler et al. [105] and Bousman et al. [108] revealed a dependence of flow pattern transitions on tube diameter. In reduced gravity, bubbles in the 40-mm diameter tube of Colin et al. were concentrated more in the central region of the tube, compared to a more uniform distribution in the smaller tubes of Dukler et al. and Bousman et al. This behavior was attributed to greater turbulence in the larger tube causing increased bubble coalescence. Colin et al. [110] showed bubbles produce maximum concentration along the center of the tube in $\mu g_e$ compared to near

the wall in 1 $g_e$. They also observed bubbly–slug transition to occur at a lower transitional void fraction of $\alpha = 0.20$, for which Eq. (14) becomes

$$j_f = 3.2 j_g. \tag{17}$$

Later, Colin et al. [112] proposed the dimensionless parameter $N_D = \sigma D/(\rho_f v_f^2) = Re^2/We$ to ascertain the influence of tube diameter and fluid properties on bubbly–slug transition.

Lee [114,115] also developed flow pattern transitional models for $\mu g_e$. Though intended for condensation, the same models were later adopted by several investigators in conjunction with adiabatic two-phase flow. Formulation of these models is based on the premise that the transitions are dictated by forces dominating each flow pattern, including surface tension, gravity, fluid inertia, friction, and turbulent fluctuations. They postulated that bubbly–slug transition is dominated by the surface tension force tending to preserve Taylor bubbles in slug flow, and turbulent fluctuations to rupture the liquid–vapor interface to form smaller bubbles. On the other hand, vapor inertia and surface tension dictated the slug–annular transition.

Reinarts [116] conducted two-phase flow experiments with R-12 in two horizontal tubes with diameters of 4.7 and 10.5 mm. Tests were conducted aboard NASA's KC-135 aircraft to simulate $\mu g_e$ as well as Lunar (1.7 m/s$^2$) and Martian (3.7 m/s$^2$) environments, and were compared with 1-$g_e$ ground tests. The influence of body force was prevalent in Lunar and Martian tests in the form of stratified and plug flow patterns not observed in $\mu g_e$, where only bubbly, slug, and annular flows were observed. Reinarts developed flow pattern transition models based on formulations proposed earlier by Lee [114,115].

More recently, several additional efforts were undertaken to capture adiabatic two-phase flow regimes in $\mu g_e$, and to predict flow pattern transitions using a variety of models and dominant dimensionless groups [117–121].

Another key focus of adiabatic microgravity studies is two-phase pressure drop. The total pressure drop in two-phase flow is composed of frictional, accelerational, and gravitational components. Notice that the accelerational component is zero for adiabatic flow. Also, the gravitational component is zero in $\mu g_e$. Therefore, adiabatic two-phase flow experiments in microgravity enable the measurement of the frictional component alone.

Because of the aforementioned concentration of bubbles along the center of large diameter tubes with almost pure liquid flow near the wall, Colin et al. [109] showed $\mu g_e$ wall friction data agree well with predictions of the Blasius correlation for single-phase turbulent flow. On the other hand, Colin et al. [111,112] detected an increase in wall friction for low Reynolds numbers in smaller tubes from single-phase relations, which was attributed to the small diameters causing bubbles to approach the wall. Zhao and Rezkallah [122] also observed an increase in wall friction at low flow rates, fostering bubbly and slug flows.

Bousman [106] found the Homogeneous Equilibrium Model (HEM) and separated flow model (SFM) incapable of accurately predicting the majority of their pressure drop data corresponding to the bubbly and slug flow regimes. However, the Lockhart–Martinelli model [123] provided fairly good predictions of annular flow data.

Both Chen et al. [124] and Choi et al. [104] showed pressure drop in $\mu g_e$ is significantly larger than in 1 $g_e$. Zhao et al. [125] showed classical 1-$g_e$ empirical pressure drop models yield poor predictions of $\mu g_e$ data. Such deviations, which demonstrate the fundamental differences in two-phase behavior between $\mu g_e$ and 1 $g_e$, have prompted investigators to devise new correlations or modified models specific to microgravity.

### 4.3. Flow boiling studies

#### 4.3.1. Two-phase flow boiling patterns and transitions

Although microgravity flow boiling experiments have been conducted since the early 1960s, far fewer studies have investigated flow boiling than pool boiling and adiabatic two-phase flow. The earliest investigations of microgravity flow boiling are attributed to Feldmanis [126] and Papell [127,128]. Table 2 provides a summary of more recent studies concerning this topic. Overall, these studies show striking differences in interfacial behavior and heat transfer mechanisms between $\mu g_e$ and 1 $g_e$.

Misawa [129] investigated subcooled and saturated flow boiling of R-113 in both drop tower (1.25 s at 0.02 $g_e$) and NASA's Learjet experiments. Using a film heated square channel ($A = 5 \times 5$ mm$^2$, $L = 500$ mm), and two electrically heated coiled tubes ($D = 4$ and 12.8 mm, $L = 500$ and 480 mm), flow patterns were shown to transition earlier in $\mu g_e$ compared to 1 $g_e$, but differences in flow behavior diminished at high vapor quality. They identified bubbly, slug, slug–frothy, annular and annular-frothy patterns, whose transitions were in good agreement with the $\mu g_e$ maps of Dukler et al. [105] and Colin et al. [109].

Saito et al. [130] performed parabolic flight water flow boiling experiments in a $25 \times 25$ mm$^2$ and 600-mm long square channel that was fitted with an electrically heated rod ($D = 8$ mm, $L = 200$ mm) along its central axis. Fig. 11(a) shows differences in interfacial behavior between $\mu g_e$ and 1 $g_e$ tests. Notice how body force effects are prevalent at 1 $g_e$ and low flow rates, where bubbles generated on the heated rod detached and stratified in the upper portion of the flow channel. On the other hand, the absence of buoyancy in $\mu g_e$ subdued bubble detachment, causing bubbles to continue to propagate along the heated surface and to grow from downstream bubble generation as well as coalescence with neighboring bubbles.

Ohta et al. [131] conducted parabolic flight microgravity flow boiling experiments using R-113 in 8-mm diameter pyrex tubes coated internally with thin heating gold film ($L = 70$ and 255 mm). Experimental data for subcooled and saturated inlet conditions were obtained for $\mu g_e$ and 2 $g_e$, and compared with 1 $g_e$ vertical upflow tests. As shown in Fig. 11(b), bubbly flow was observed in all gravity levels for subcooled inlet conditions and relatively low mass velocity of $G = 150$ kg/m$^2$ s. And like $\mu g_e$ pool boiling, bubbles in $\mu g_e$ flow boiling were significantly larger than in 1 $g_e$ and 2 $g_e$. But for the highest mass velocity of $G = 600$ kg/m$^2$ s, similar bubble detachment diameters were observed for all gravity levels. This similarity was attributed to increased fluid inertia dwarfing body force effects by providing sufficient interfacial shear to detach bubbles from the heated surface before further growth due to evaporation could take effect. Fig. 11(b) shows body force effects were also suppressed for high inlet quality and high heat flux conditions, where similar annular flow behavior was observed for all gravity levels.

Celata et al. performed multiple parabolic flight experiments to investigate flow boiling [134] and quenching [139,140] in $\mu g_e$. Their flow boiling experiments involved subcooled FC-72 introduced through circular glass tubes ($D = 4$ and 6 mm) that were heated by metallic tape helically coiled on their outer surfaces. Interfacial behavior in $\mu g_e$ for the 4-mm tube agreed with that for 1-$g_e$ vertical upflow, where bubbly flow was encountered at low mass velocities and low heat fluxes. They speculated that the absence of buoyancy in $\mu g_e$ prolonged bubble growth during nucleation, resulting in larger bubble detachment diameters compared to 1-$g_e$. Intermittent (plug–slug) flow patterns were achieved with an increase in heat flux in $\mu g_e$, whereas churn flow was observed at 1 $g_e$ for the same conditions. Overall, similar interfacial behavior was observed at high mass velocities and high heat fluxes, indicating independence of body force effects, and the observed

**Table 2**
Summary of prior reduced gravity flow boiling studies.

| Author(s) | Microgravity platform | Test fluid | Flow/heater geometry | Test conditions | Remarks |
|---|---|---|---|---|---|
| Papell (1964) [128] | Parabolic flight (NASA Learjet) | Water | Circular (nickel-alloy) $D$ = 7.9 mm, $L$ = 165.1 mm, vertical | $p$ = 3.4 bar<br>$\Delta T_{sub}$ = 79.4–92.2 °C<br>$\dot{m}$ = 0.09 kg/s<br>$q''$ = 2289.6 kW/m$^2$ | – Flow patterns observed in $\mu g_e$: bubbly and slug |
| Misawa (1993) [129] | Drop tower (University of Florida) (0.02 $g_e$, 1.25 s) | R-113 | Rectangular (Pyrex) $A$ = 5 × 5 mm$^2$, $L$ = 500 mm, $CL_2Sn$ film heater on 4 sides | $\Delta T_{sub}$ = 4.6–16.9 °C<br>$G$ = 37.7–114.4 kg/m$^2$ s<br>$q''$ = 2.9 kW/m$^2$<br>$x_{e,o}$ = −0.045–0.175 | – Flow patterns observed in $\mu g_e$: bubbly, slug, slug–frothy, annular, annular-frothy<br>– Bubbles significantly larger in $\mu g_e$ than 1 $g_e$<br>– Flow pattern transition occurs at smaller values of void fraction in $\mu g_e$ than 1 $g_e$<br>– Data agree well with flow pattern transitional maps of Dukler et al. [105] and Colin et al. [109]<br>– Void fraction rapidly increases in subcooled region in $\mu g_e$ compared to 1 $g_e$<br>– Heat transfer deteriorates in $\mu g_e$ compared to 1 $g_e$<br>– For bubbly flow, turbulence generated by bubbles is weakened in $\mu g_e$<br>– Wall shear stress in $\mu g_e$ is 1.18 times larger than in 1 $g_e$ due to large bubbles in low-quality region<br>– Homogeneous model predicts bubbly flow pressure drop well |
| Saito et al. (1994) [130] | Parabolic flight (MU-300) | Water | Rectangular $A$ = 25 × 25 mm$^2$, $L$ = 600 mm, rod-type electric heater, $D$ = 8 mm, $L$ = 200 mm, horizontal | $p$ = 90–204 kPa<br>$T_{in}$ = 86.1–112.8 °C<br>$U$ = 3.7–22.9 cm/s<br>$q''$ = 5.3–18.6 W/cm$^2$ | – In 1 $g_e$ at low inlet flow velocity and high heat flux, bubbles detach frequently from heated rod then stratify in upper portion of flow channel due to buoyancy<br>– Stratification is not observed in $\mu g_e$ due to minimal detachment of bubbles, which propagate along heated rod, continuously growing and coalescing with neighboring bubbles, especially at low inlet velocity, low inlet subcooling, and high heat flux |
| Ohta (1997) [131] | Parabolic flight (MU-300) | R-113 | Circular (Pyrex) $D$ = 8 mm, 100- and 300-mm long, $L$ = 70 and 255 mm, gold film heater (0.01 μm), vertical upflow | $p$ = 0.11–0.22 MPa<br>$G$ = 150–600 kg/m$^2$ s<br>$x_{e,in}$ = 0–0.8<br>$q''$ = 5–150 kW/m$^2$ | – Heat transfer regimes in $\mu g_e$ are segregated based on mass velocity, heat flux, and quality, with the relative significance of body force identified for each regime |
| Ma and Chung (2001) [132] | Drop tower (Washington State University) ($10^{-3}$ $g_e$, 2.1s) | FC-72 | Square (Pyrex) $A_h$ = 1 × 1 mm$^2$ gold film heater (0.045 μm), horizontal | $p$ = 112 kPa<br>$T_{in}$ = 30 °C<br>$\Delta T_{sub,in}$ = 26 °C<br>$U$ = 6.5–30 cm/s<br>$q''$ = 5.4, 39.7 kW/m$^2$ | – Bubbles are larger and acquire semi-spherical shape on heated surface in $\mu g_e$ compared to 1 $g_e$<br>– In $\mu g_e$, increasing flow rate suppresses growth of bubble before departure because of dominance of convective heat loss at exposed liquid–vapor interface compared to evaporation rate at bubble base<br>– In 1 $g_e$, greater frequency of bubble generation increases with increasing flow rate compared to $\mu g_e$, but this difference is minimal at very high flow rates ($Re \geqslant 16{,}821$) |
| Ma and Chung (2001) [132] | Drop tower (Washington State University) ($10^{-3}$ $g_e$, 2.1 s) | FC-72 | Platinum wire $D$ = 0.254 mm, $L$ = 20 mm, horizontal | $p$ = 112 kPa<br>$T_{in}$ = 30 °C<br>$\Delta T_{sub,in}$ = 26 °C<br>$U$ = 6.5–30 cm/s<br>$q''$ = 0–600 kW/m$^2$ | – Heat transfer enhancement is greater in $\mu g_e$ at lower flow rates<br>– Degradation in heat transfer occurs in transition boiling regime up to CHF in $\mu g_e$, resulting in significantly lower CHF compared to 1 $g_e$ |
| Westheimer and Peterson (2001) [133] | Parabolic flight (NASA KC-135) | R-113 | Circular (Borosilicate glass) annular countercurrent heat exchanger, $D$ = 10 mm, $L$ = 584 mm, vertical upflow | $p$ = ambient<br>R-113: $Q$ = 100 mL/min<br>Water: $Q$ = 24 mL/min<br>R-113: $q$ = 0–11 W<br>Water: $q$ = 266–356 W | – Flow patterns observed in $\mu g_e$: bubble, slug and annular<br>– Bubble speed decreases in $\mu g_e$ due to absence of buoyancy<br>– Lower heat input is required to initiate flow regime transition in $\mu g_e$<br>– 1-$g_e$ flow pattern maps predict experimental data poorly<br>– Highest local heat transfer coefficient is achieved at axial location corresponding to transition from bubbly to slug flow |
| Celata et al. (2007) [134] | Parabolic flight (Zero-G Airbus A300) | FC-72 | Circular (Pyrex) $D$ = 4.0 and 6.0 mm, $L$ = 165 and 145 mm, Joule effect through metallic tape, vertical upflow | $p$ = 1.6–1.8 bar<br>$\Delta T_{sub,in}$ = 9–30 °C<br>$G$ = 47.5–520 kg/m$^2$s<br>$q'' \leqslant 100$ kW/m$^2$<br>$x_{e,o} \leqslant 0.22$ | – Flow patterns observed in $\mu g_e$: bubbly, intermittent (slug–plug) and annular<br>– Flow pattern map of Dukler et al. [105] shows reasonable agreement with $\mu g_e$ data for 4.0 mm tube<br>– Modified criterion based on Dukler et al. [105] map is proposed to correlate $\mu g_e$ data for 6.0 mm tube |
| Luciani et al. (2008) [135] | Parabolic flight (A300) | HFE-7100 | Rectangular (Inconel) $D_h$ = 0.49, 0.84, 1.18 mm, $H/W$ = 0.04–0.11, $L$ = 50 mm, vertical upflow | $T_{sat}$ = 54 °C<br>$\Delta T_{sub,in}$ = 2 °C<br>$\dot{m}$ = 0.26 g/s<br>$q''$ = 33 kW/m$^2$ | – Heat transfer is enhanced in $\mu g_e$<br>– For all gravity conditions tested ($\mu g_e$, 1 $g_e$, 1.8 $g_e$), two-phase heat transfer coefficient is highest at the inlet and decreases in the flow direction<br>– No noticeable difference observed between 1 $g_e$ and 1.8 $g_e$ data |

(*continued on next page*)

**Table 2** (*continued*)

| Author(s) | Microgravity platform | Test fluid | Flow/heater geometry | Test conditions | Remarks |
|---|---|---|---|---|---|
| Baltis et al. (2012) [136] | Parabolic flight (Zero-G Airbus A300) | FC-72 | Circular (Pyrex) $D$ = 2.0, 4.0, 6.0 mm, $L$ = 0.2 m Joule effect through metallic tape | $p$ = 1.2–1.8 bar<br>$\Delta T_{sub,in}$ = −9—30 °C<br>$G$ = 47.5–570.0 kg/m$^2$s<br>$q''\leqslant$ 100.0 kW/m$^2$<br>$x_{e,o}\leqslant$ 0.22 | – Bubbly flow pattern exhibits heat transfer enhancement predominantly at the tube inlet, which is degraded at the outlet<br>– Increasing vapor quality and/or mass velocity diminishes body force effects<br>– The largest tube tested ($D$ = 6.0 mm) shows body force effects are dominant for $G$ < 425 kg/m$^2$ s<br>– Smaller tubes show diminishing influence of body force, but greater flow instabilities occur in the smallest tube ($D$ = 2.0 mm) |
| Brutin et al. (2013) [137] | Parabolic flight (A300) | HFE-7100 | Rectangular (Inconel) $D_h$ = 0.84 mm, $H/W$ = 0.08, $L$ = 50 mm, vertical upflow | $T_{sat}$ = 54 °C<br>$\Delta T_{sub,in}$ = 2 °C<br>$G$ = 30–248 kg/m$^2$s<br>$q''$ = 15–55 kW/m$^2$ | – Up to 50% deterioration of frictional pressure drop is achieved in $\mu g_e$ compared to 1 $g_e$, the pressure drop in 1.8 $g_e$ is 1.3 times higher than in 1 $g_e$<br>– Local two-phase heat transfer coefficient is enhanced in $\mu g_e$ due to smaller film thickness |
| Narcy et al. (2013) [138] | Parabolic flight | HFE-7000 | Circular (sapphire) $D$ = 6 mm, $L$ = 200 mm, ITO film heater, vertical upflow | $P$ = 1–2 bar<br>$G$ = 50–1200 kg/m$^2$ s<br>$q''\leqslant$ 45 kW/m$^2$<br>$x_{e,in}\leqslant$ 0.9 | – Flow patterns observed in $\mu g_e$: bubbly, slug and annular flow<br>– Bubbly and slug flows transition to annular flow earlier in $\mu g_e$ than in 1 $g_e$ due to increased bubble coalescence<br>– Thinner liquid film is measured in annular flow and transitional flow (slug-to-annular region) in $\mu g_e$ compared to 1 $g_e$<br>– Adiabatic pressure drop downstream of the heated section is correlated well for bubbly and annular flow using the Lockhart–Martinelli [123] correlation<br>– At low mass velocity, the two-phase heat transfer coefficient is degraded in $\mu g_e$ compared to 1 $g_e$ for $x_e$ < 0.2, and enhanced for $x_e$ > 0.2 |

interfacial behavior and heat transfer characteristics were similar to those of Ohta et al. [131]. Similar flow patterns were observed by Celata et al. in the 6.0-mm tube with the exception of annular flow. For bubbly flow in $\mu g_e$, this larger tube promoted greater bubble nucleation, which enhanced coalescence frequency and led to the formation of larger bubbles. Transition from bubbly to intermittent flow occurred at lower heat fluxes in $\mu g_e$ compared to 1 $g_e$. Celata et al. also explored the effectiveness of prior $\mu g_e$ flow pattern maps in predicting their own data. The transitional criteria proposed by Dukler et al. [105] showed good agreement with their 4.0-mm tube data.

Luciani et al. [135,141] investigated subcooled flow boiling of HFE-7100 in three narrow rectangular channels ($6.0 \times 0.254$, $6.0 \times 0.454$, $6.0 \times 0.654$ mm$^2$) with a heated length of 50 mm. Tests were conducted in parabolic flight to simulate $\mu g_e$ and 1.8 $g_e$, and later compared with 1-$g_e$ vertical upflow tests. They detected some upstream heat transfer enhancement in $\mu g_e$, but similar interfacial behavior in 1 $g_e$ and 1.8 $g_e$.

#### 4.3.2. Two-phase heat transfer and pressure drop

Misawa [129] investigated the contributions of turbulence in bubbly flow. Because of the absence of drift in $\mu g_e$, they postulated that turbulence induced by bubble agitation is compromised, leading to deterioration in heat transfer in $\mu g_e$ compared to 1 $g_e$.

Ohta et al. [131] performed flow boiling experiments in parabolic flight at $\mu g_e$ and 2 $g_e$, which they compared with ground 1 $g_e$ vertical upflow tests. They monitored wall temperature during parabolic flight in response to varying gravity. For all mass velocities fostering bubbly flow, changes in gravity during parabolic flight had minimum effects on heat transfer, suggesting a dominant nucleate boiling heat transfer mechanism for bubbly flow that is both local and confined to the heated wall. For conditions yielding annular flow with moderate inlet quality, heat transfer at low heat fluxes was governed by two-phase forced convection and strongly influenced by gravity, and heat transfer deteriorated in low-$g$ compared to high-$g$. Waves in the liquid film caused film thickness to decrease at high-$g$ and increase in $\mu g_e$. For annular flow and high heat flux, nucleate boiling was observed within the annular liquid film, yielding similar heat transfer coefficients through the varying gravity event. Yet, the influence of gravity on annular heat transfer diminished at high inlet quality, where greater shear forces resulting from increased vapor core velocity appeared to overcome body force effects.

Celata et al. [139] and Baltis et al. [136] also explored wall temperature variations in a 6.0-mm tube with varying gravity during parabolic maneuvers. At low mass velocity and low exit vapor quality, the hypergravity phase produced bubbly flow with small bubbles detaching from the wall. Entering the $\mu g_e$ phase, heat transfer was enhanced significantly in the inlet and reduced in the outlet. The upstream enhancement was attributed to greater mixing and turbulence brought about by larger bubble diameters in $\mu g_e$. With increased mass velocity, no significant variations in wall temperature were detected, proving these operating conditions greatly reduced the influence of body force. At low mass velocity and high exit quality, which yielded intermittent/annular flow, slight gravitational effects were detected.

Luciani et al. [135,141] employed inverse methods to estimate the local heat transfer coefficient. They reported heat transfer enhancement in all $\mu g_e$ conditions, with average heat transfer coefficients as much as 30% higher than terrestrial data. For all gravity levels, large heat transfer coefficients were measured near the inlet, which dropped sharply to fairly constant value from about the middle of the channel to the exit. Brutin et al. [137] continued the work of Luciani et al. by examining void fraction and frictional two-phase pressure drop. The frictional pressure drop increased with increasing gravity, which they explained by a

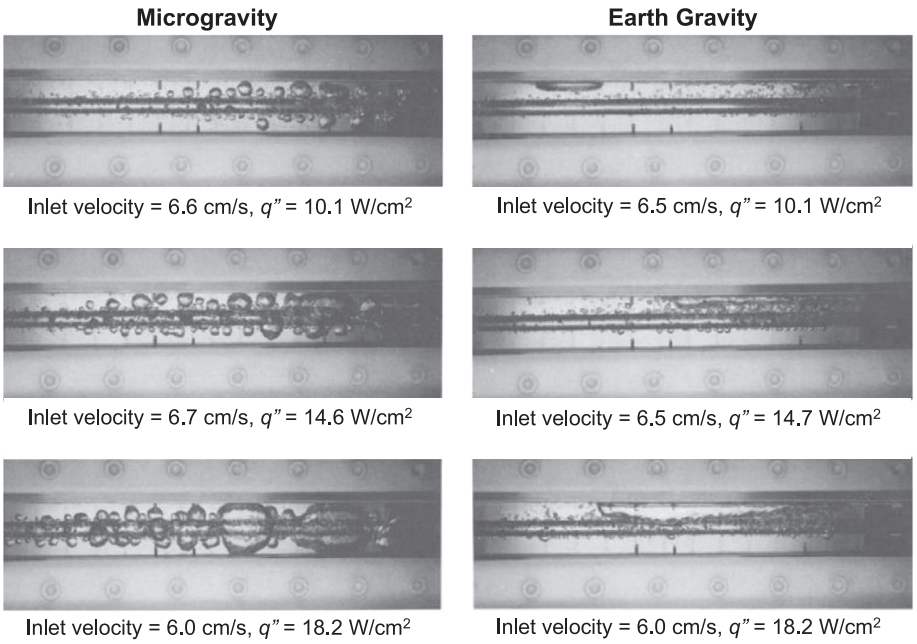


**Fig. 11.** (a) Comparison of water flow boiling behavior in microgravity and Earth gravity along a square channel fitted with a central cylindrical heating rod (adapted from Saito et al. [130]). (b) Comparison of flow boiling of R-113 in vertical upflow in 1 $g_e$, 2 $g_e$ and $\mu g_e$ for subcooled inlet conditions at low and high mass velocities, and for low mass velocity and high inlet quality (adapted from Ohta [131]).

decrease in void fraction with increasing gravity causing more of the channel cross-section to be occupied by liquid, thereby increasing friction.

Overall, the influence of body force on two-phase heat transfer appears to be highly dependent on mass velocity, inlet quality and heat flux, which also dictate flow pattern. Also, some of the findings by different investigators appear quite contradictory.

### 4.4. Flow boiling critical heat flux

As mentioned earlier, the ability to predict CHF is of paramount importance to the functionality of any heat-flux controlled flow boiling system. Also, as discussed earlier, several microgravity pool boiling studies point to an appreciable decrease in CHF in $\mu g_e$ as compared to 1 $g_e$. In the absence of a body force to remove growing vapor bubbles, this decrease was attributed mostly to bubble coalescence into an unusually large bubble encompassing the entire heated wall. Flow boiling constitutes a practical and effective means to precluding this massive vapor coalescence by relying on liquid inertia to flush bubbles away from the heated wall and providing a path for bulk liquid to replenish the heated wall. Despite these important facts, very few studies have been devoted exclusively to flow boiling CHF in reduced gravity.

Ohta [131] obtained limited flow boiling CHF measurements in $\mu g_e$ at high inlet quality, but noted that the CHF could not be accurately measured in the absence of local wall temperature measurements along the heated wall. Ma and Chung [132] investigated subcooled flow boiling of FC-72 across a heated 0.254-mm

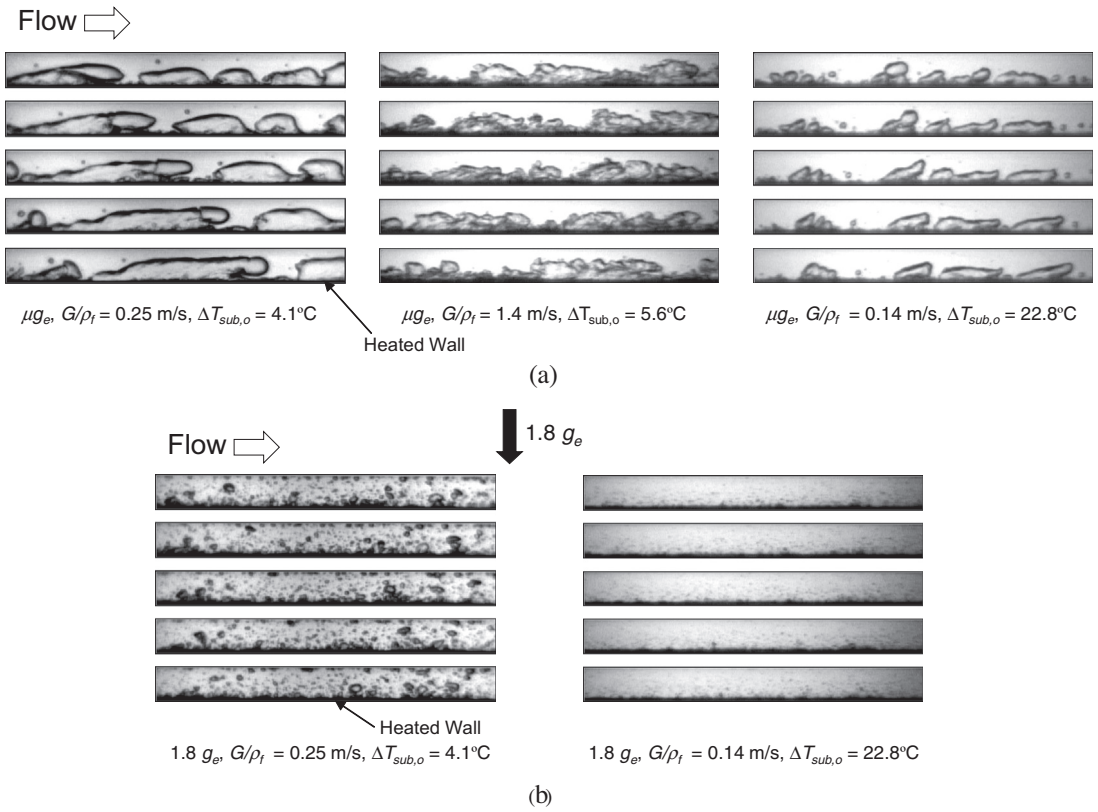


**Fig. 12.** (a) Wavy Vapor Layer CHF Regime prevalent in $\mu g_e$ at both low and high velocities as well as near saturated and subcooled conditions. (b) Low velocity pool-boiling-like flow boiling at 1.8 $g_e$ [42].

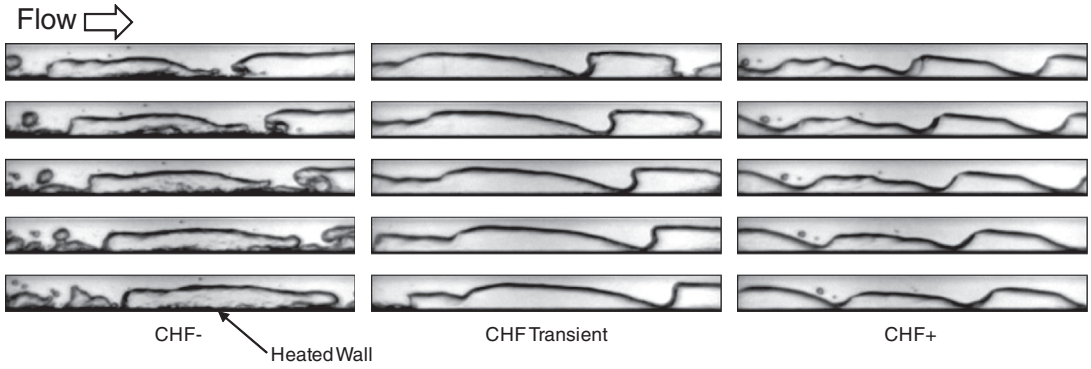


**Fig. 13.** CHF transient in $\mu g_e$ for $G/\rho_f$ = 0.15 m/s and $\Delta T_{sub,o}$ = 3.0 °C [42].

platinum wire in a 2.1-s drop tower. They measured an appreciable shift in the $\mu g_e$ boiling curve to lower heat fluxes compared to 1 $g_e$, indicating significant reduction in heat transfer effectiveness. Additionally, CHF in $\mu g_e$ was significantly lower than in 1 $g_e$. However, differences in both heat transfer rate and CHF decreased with increasing flow rate.

Zhang et al. [42] conducted subcooled flow boiling CHF experiments with FC-72 onboard NASA's KC-135 jet. CHF data were measured in $\mu g_e$, Lunar gravity (0.17 $g_e$) and Martian gravity (0.38 $g_e$), which were achieved with different parabolic maneuvers, and later compared with 1-$g_e$ CHF data. Their study featured a 2.5 × 5.0 mm$^2$ rectangular polycarbonate flow channel that was fitted on one of the 2.5-mm sides with a 101.6-mm long electrically heated copper plate. As discussed earlier in relation to Fig. 5(a) and (b), prior experiments by Zhang et al. involving flow boiling at different orientations in Earth gravity showed drastically different CHF mechanisms at low velocities, but the same wavy vapor layer behavior at high velocity regardless of orientation. Unlike this terrestrial behavior, Fig. 12(a) shows flow-boiling CHF in $\mu g_e$ follows the same mechanism at both low and high velocities. For near-saturated flow at both $G/\rho_f$ = 0.25 and 1.4 m/s, bubbles coalesced along the heated wall into vapor patches resembling a continuous wavy vapor layer. Fig. 12(a) also shows similar CHF behavior at $G/\rho_f$ = 0.14 m/s and a high subcooling of 22.8 °C.

Fig. 12(b) depicts sequential images of flow boiling at low velocities and 1.8 $g_e$ for both low and high subcooling. Because of the large buoyancy force perpendicular to the heated wall, the images to the left show bubbles being removed from the surface before they have the opportunity to coalesce, and boiling behavior seems to mimic pool boiling at 1 $g_e$. The images to the right show high subcooling reduces the size of vapor bubbles considerably during growth and detachment as a result of strong condensation effects.

Zhang et al. [42] also conducted a few $\mu g_e$ tests in which high-speed video imaging captured interfacial behavior during the CHF transient. Fig. 13 shows for $G/\rho_f = 0.15$ m/s and $\Delta T_{sub,o} = 3$ °C, how, just before CHF, vapor patches grow into a wavy vapor layer that propagates along the wall as vigorous boiling in wetting fronts between the vapor patches maintains heat transfer from the heated wall to the liquid. Notice the wetting front in the middle images beginning to lift off from the heated wall as the CHF transient progresses. This lift-off triggered a chain reaction in which upstream wettings fronts began to detach from the surface, as depicted in the right images, until the entire heated wall was engulfed in a continuous insulating wavy vapor layer. This behavior is consistent with the Interfacial Lift-off CHF Model originally proposed by Galloway and Mudawar [25,26].

The Interfacial Lift-off Model uses hydrodynamic instability to describe the wavy interface between a liquid layer of mean velocity $U_f$ and mean thickness $H_f$, and a vapor layer of mean velocity $U_g$ and mean thickness $H_g$, as shown in Fig. 14(a). Wetting front formation requires that the interfacial wavelength exceed the critical wavelength, $\lambda_c$, which is given by

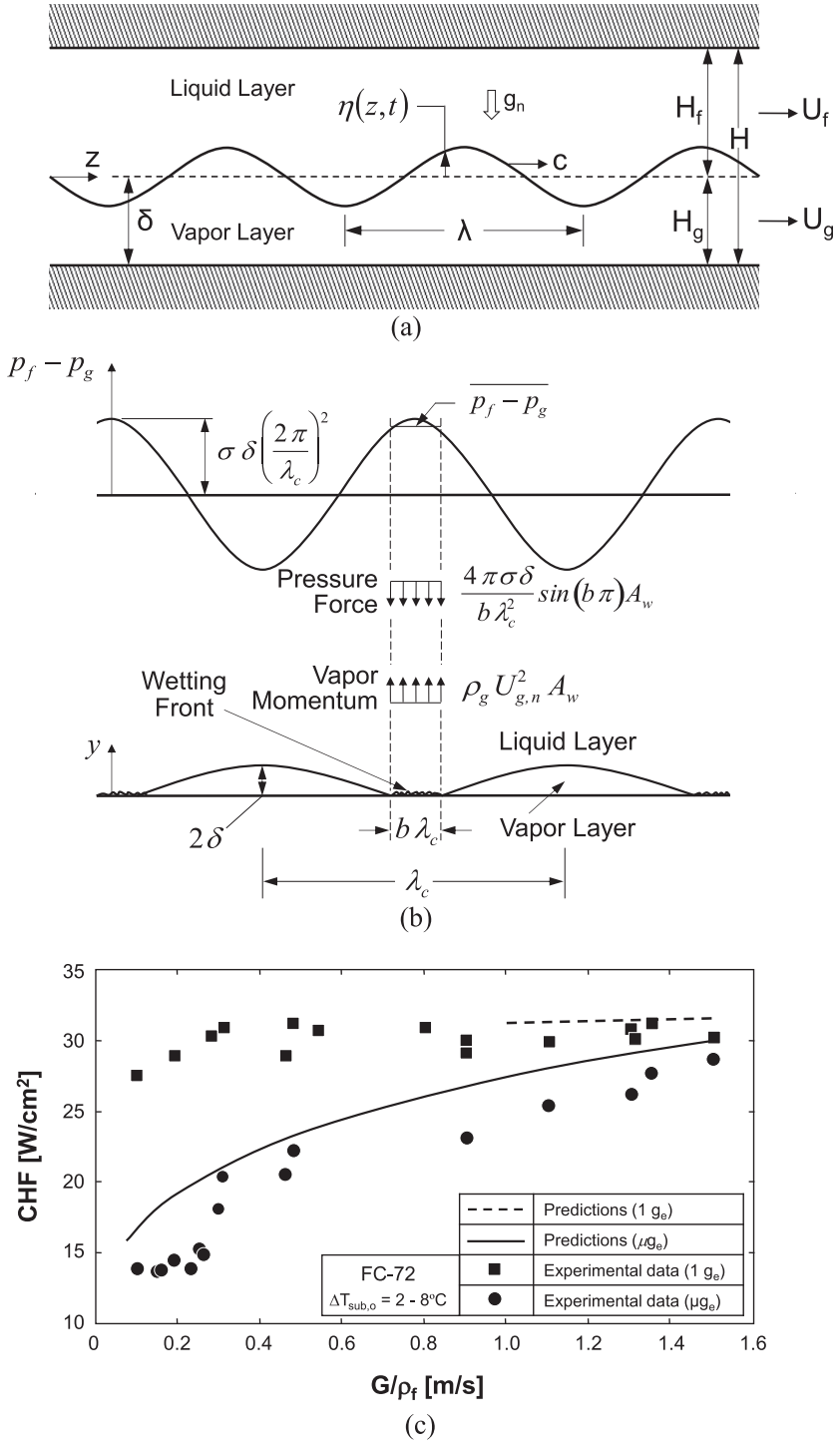


**Fig. 14.** (a) Wavy interface between liquid and vapor layers [58]. (b) Interfacial Lift-off of wetting front at CHF [58]. (c) Comparison of CHF data and Interfacial Lift-off Model predictions for $\mu g_e$ and horizontal 1 $g_e$ flow boiling [42].

$$k_c = \frac{2\pi}{\lambda_c} = \frac{\rho_f''\rho_g''(U_g - U_f)^2}{2\sigma(\rho_f'' + \rho_g'')} + \sqrt{\left[\frac{\rho_f''\rho_g''(U_g - U_f)^2}{2\sigma(\rho_f'' + \rho_g'')}\right]^2 + \frac{(\rho_f - \rho_g)g_n}{\sigma}}, \quad (18)$$

where $\rho_f'' = \rho_f \coth(kH_f)$ and $\rho_g'' = \rho_g \coth(kH_g)$ are 'modified density' terms, and $g_n$ is the component of gravity perpendicular to the heated wall. Eq. (18) proves large velocity differences tend to destabilize the interface, while surface tension helps preserve interfacial stability. Depending on flow orientation relative to gravity, body force can be stabilizing or destabilizing.

The second part of the Interfacial Lift-off Model concerns the process of separation of wetting fronts from the wall, which is the trigger mechanism for CHF. Notice that the curvature of the liquid–vapor interface produces a pressure force that promotes interfacial contact with the heated wall, which is the process necessary for maintaining liquid replenishment. CHF occurs when the normal momentum of vapor generated in the wetting front just exceeds the pressure force. For an interfacial wave of the form $\eta(z,t) = \eta_o e^{i\,k\,(z-ct)}$, pressure difference perpendicular to the wall is expressed as

$$p_f - p_g = -\left[\rho_f''(c - U_f)^2 + \rho_g''(c - U_g)^2 + (\rho_f - \rho_g)\frac{g_n}{k}\right] k\eta_0 e^{ik(z-ct)}. \quad (19)$$

Assuming the wetting front occupies a fixed fraction $b$ of the critical wavelength, the average pressure force for a wetting front is determined by averaging the pressure difference over $b\lambda_c$.

$$\overline{p_f - p_g} = \frac{4\pi\sigma\delta}{b\lambda^2}\sin(b\pi), \quad (20)$$

where $\delta$ is the mean vapor layer thickness. Fig. 14(b) shows the pressure force is opposed by vapor momentum $\rho_g U_{g,n}^2$ emanating from the wetting front normal to the heated wall.

Using extensive video records and statistical averaging techniques, Sturgis and Mudawar [27,28] showed that $b = 0.2$ over a broad range of flow conditions. They detected a continuous wetting region of length $z^*$, defined as $z^* = z_o + \lambda_c(z^*)$, where $z_o$ is the distance from the leading edge of the heated wall to the location where $U_g$ just surpasses $U_f$. The wavy interface is therefore generated at $z^*$ and propagates downstream.

Considering flow boiling with a subcooled inlet, the heat concentrated in a wetting front is consumed by vaporizing liquid, $q_w'' A_w = (c_{p,f}\Delta T_{sub,in} + h_{fg})\rho_g U_{g,n} A_w$, where $A_w$ is the wetting front area. The local heat flux required to push the interface away from the wall is determined by equating the vapor momentum, $\rho_g U_{g,n}^2$, to the pressure force obtained from Eq. (20).

$$q_w'' = \rho_g(c_{p,f}\Delta T_{sub,i} + h_{fg})\sqrt{\frac{\overline{p_f - p_g}}{\rho_g}} = \rho_g(c_{p,f}\Delta T_{sub,in} + h_{fg})\left[\frac{4\pi\sigma}{\rho_g}\frac{\sin(b\pi)}{b}\right]^{1/2}\left.\frac{\delta^{1/2}}{\lambda_c}\right|_{z^*}. \quad (21)$$

The critical heat flux, $q_m''$, is defined as the average heat flux over the entire heated area, which is related to the wetting front heat flux by the relation $q_m'' = bq_w''$. This gives the following analytical expression for CHF corresponding to subcooled inlet conditions.

$$q_m'' = \rho_g(c_{p,f}\Delta T_{sub,in} + h_{fg})\left[\frac{4\pi\sigma b\sin(b\pi)}{\rho_g}\right]^{1/2}\left.\frac{\delta^{1/2}}{\lambda_c}\right|_{z^*}. \quad (22)$$

Notice that $\delta$ and $\lambda_c$ in Eq. (22) are calculated at $z^*$. These two parameters are determined from a separated flow model that is used to predict $U_f(z)$, $U_g(z)$, and $\delta(z)$. Table 3 provides detailed relations for the separated flow model.

**Table 3**
Summary of separated flow model relations [58].

Quality and area fraction relations:
$x_e = \frac{\rho_g U_g \alpha}{G}$, $\alpha = \frac{\delta}{H}$, $A = H \times W$ (channel height × channel width)
Momentum conservation:
$G^2 \frac{d}{dz}\left[\frac{(1-x_e)^2}{\rho_f(1-\alpha)}\right] = -(1-\alpha)\frac{dp}{dz} - \frac{\tau_{wf}P_{wf}}{A} + \frac{\tau_i P_i}{A} - \rho_f(1-\alpha)g_{II}$
$G^2 \frac{d}{dz}\left(\frac{x_e^2}{\rho_g \alpha}\right) = -\alpha\frac{dp}{dz} - \frac{\tau_{wg}P_{wg}}{A} - \frac{\tau_i P_i}{A} - \rho_g \alpha g_{II}$
Wall shear stress relations ($k$ = $g$ or $f$): $\tau_{w,k} = \frac{1}{2}\rho_k U_k^2 f_k$
$f_k = 0.184\left(\frac{\rho_k U_k D_{h,k}}{\mu_k}\right)^{-1/5}$
Interfacial shear stress:
$\tau_i = \frac{C_{f,i}}{2}\rho_g(U_g - U_f)^2$
where $C_{f,i} = 0.5$

Fig. 14(c) shows variations of the CHF data of Zhang et al. with velocity in $\mu g_e$ and l $g_e$. In $\mu g_e$, CHF increases appreciably with increasing velocity. However, this dependence is far weaker at l $g_e$. At the lowest velocity, CHF in $\mu g_e$ is only 50% of that at 1 $g_e$. Increasing velocity is shown reducing differences between the two gravitational environments, with the CHF data converging around 1.5 m/s. Also included in Fig. 14(c) are CHF predictions based on the Interfacial Lift-off Model. Notice that this model provides predictions for $\mu g_e$ over the entire velocity range, while only high velocity predictions are possible for 1 $g_e$ because horizontal flow at lower velocities at 1 $g_e$ is associated with the 'Pool Boiling' CHF regime, Fig. 5(a), which is fundamentally different from the Wavy Vapor Layer Regime for which the model is intended. The CHF predictions point to very important implications to future space missions. First, unlike 1 $g_e$, CHF in $\mu g_e$ is dominated by the Wavy Vapor Layer Regime regardless how small is the flow velocity. Second, flow boiling CHF in $\mu g_e$ can be accurately predicted by the Interfacial Lift-off Model. Third, convergence of $\mu g_e$ and 1 $g_e$ data at about 1.5 m/s proves it is possible to design inertia-dominated space systems by maintaining flow velocities above this velocity threshold. Inertia-dominated systems allow data, correlations, and/or models developed at 1 $g_e$ to be safely implemented in the design of space systems.

## 5. Concluding remarks

This study reviewed published literature concerning two-phase flow and heat transfer in reduced gravity. Discussed are the different methods and platforms dedicated to exploring the influence of reduced gravity, including ground flow boiling experiments performed at different orientations relative to Earth gravity, as well as adiabatic two-phase flow, pool boiling, flow boiling and CHF reduced gravity experiments. Key observations from this review can be summarized as follows.

(1) Despite the important fundamental knowledge gained from microgravity pool boiling experiments, there is general agreement that, because of unusually large bubble size and appreciable reduction in CHF compared to terrestrial data, pool boiling will be difficult to implement in future space applications.
(2) By relying on fluid inertia to overcome body force effects, flow boiling provides an effective means for controlling bubble growth and sustaining liquid replenishment of the heater surface to boast CHF. This renders flow boiling a very suitable cooling configuration for future space applications.
(3) Many of the published microgravity heat transfer databases are measured using heater designs that fail to satisfy the asymptotic wall thickness limit, and therefore produce measurements that are heater specific rather than represent metallic surfaces of practical interest.

(4) Despite the extensive microgravity data and flow visualization results available in the literature, there is a severe shortage of useful correlations, mechanistic models and/or computational models, which compromises readiness to adopt flow boiling in future space systems.
(5) Emphasis in future microgravity studies should be placed on operating conditions, particularly mass velocity, that ensure inertia-dominated performance independent of gravity. Exceeding the minimum mass velocity necessary to achieve this goal allows data, correlations, and/or models developed at 1 $g_e$ to be safely implemented in the design of space systems.
(6) Most reduced gravity experiments have been performed in short duration drop tower, drop shaft or parabolic flight platforms. Lack of ability to achieve steady state in short duration experiments brings into question the validity of a significant portion of this literature. Following the retirement of NASA's Space Shuttle program, the ISS constitutes the ideal testing platform for future flow boiling experiments. However, ISS experiments are very complex and costly, and require many years of development and safety certification. To maximize return on investment in space research, future ISS flow boiling experiments will require close cooperation among space agencies worldwide on the design of ISS facilities, performance of experiments, sharing of data, and development of predictive correlations and models.
(7) Emphasis should also be placed on microgravity fluid flow and heat transfer associated with condensation, which is expected to be used concurrently with flow boiling in future space thermal management systems.

## Conflict of interest

None declared.

## Acknowledgement

The authors are grateful for the partial support of the National Aeronautics and Space Administration (NASA) under Grants NNX13AB01G and NNX13AC83G.

## References

[1] I. Mudawar, Two-phase micro-channel heat sinks: theory, applications and limitations, J. Electron. Packag. – Trans. ASME 133 (2011). 041002-2.
[2] T.M. Anderson, I. Mudawar, Microelectronic cooling by enhanced pool boiling of a dielectric fluorocarbon liquid, J. Heat Transfer – Trans. ASME 111 (1989) 752–759.
[3] R.L. Webb, The evolution of enhanced surface geometries for nucleate boiling, Heat Transfer Eng. 2 (1981) 46–69.
[4] D.D. Hall, I. Mudawar, Critical heat flux (CHF) for water flow in tubes – I. Compilation and assessment of world CHF data, Int. J. Heat Mass Transfer 43 (2000) 2573–2604.
[5] D.D. Hall, I. Mudawar, Critical heat flux (CHF) for water flow in tubes – II. Subcooled CHF correlations, Int. J. Heat Mass Transfer 43 (2000) 2605–2640.
[6] H.J. Lee, S.Y. Lee, Heat transfer correlation for boiling flows in small rectangular horizontal channels with low aspect ratios, Int. J. Multiphase Flow 27 (2001) 2043–2062.
[7] L. Lin, R. Ponnappan, Heat transfer characteristics of spray cooling in a closed loop, Int. J. Heat Mass Transfer 46 (2003) 3737–3746.
[8] M. Visaria, I. Mudawar, Theoretical and experimental study of the effects of spray orientation on two-phase spray cooling and critical heat flux, Int. J. Heat Mass Transfer 51 (2008) 2398–2410.
[9] Y. Katto, M. Kunihiro, Study of the mechanism of burn-out in boiling system of high burn-out heat flux, Bull. JSME 16 (1973) 1357–1366.
[10] D.C. Wadsworth, I. Mudawar, Enhancement of single-phase heat transfer and critical heat flux from an ultra-high-flux-source to a rectangular impinging jet of dielectric liquid, J. Heat Transfer – Trans. ASME 114 (1992) 764–768.
[11] M.E. Johns, I. Mudawar, An ultra-high power two-phase jet-impingement avionic clamshell module, J. Electron. Packag. – Trans. ASME 118 (1996) 264–270.
[12] M.K. Sung, I. Mudawar, Experimental and numerical investigation of single-phase heat transfer using a hybrid jet-impingement/micro-channel cooling scheme, Int. J. Heat Mass Transfer 49 (2006) 682–694.
[13] M.K. Sung, I. Mudawar, Correlation of critical heat flux in hybrid jet impingement/micro-channel cooling scheme, Int. J. Heat Mass Transfer 49 (2006) 2663–2672.
[14] F.P. Chiaramonte, J.A. Joshi, Workshop on critical issues in microgravity fluids, transport, and reaction processes in advanced human support technology – final report, NASA TM-2004-212940, 2004.
[15] The National Academies, Recapturing a Future for Space Exploration: Life and Physical Sciences Research for a New Era, National Academies Press, Washington, DC, 2011.
[16] H. Lee, I. Mudawar, M.M. Hasan, Experimental and theoretical investigation of annular flow condensation in microgravity, Int. J. Heat Mass Transfer 61 (2013) (2013) 293–309.
[17] N.J. Penley, C.P. Schafer, J.D.F. Bartoe, The international space station as a microgravity research platform, Acta Astronaut. 50 (2002) 691–696.
[18] F. Incropera, D. Dewitt, T. Bergman, A. Lavine, Fundamentals of Heat and Mass Transfer, sixth ed., Wiley, Hoboken, NJ, 2007.
[19] I. Mudawar, Recent advances in high-flux, two-phase thermal management, J. Therm. Sci. Eng. Appl. – Trans. ASME 5 (2013) 021012.
[20] S.S. Kutateladze, A.I. Leont'ev, Some applications of the asymptotic theory of the turbulent boundary layer, in: Proc. 3rd Int. Heat Transfer Conf., vol. 3, Chicago, Illinois, 1966, pp. 1–6.
[21] L.S. Tong, Boundary-layer analysis of the flow boiling crisis, Int. J. Heat Mass Transfer 11 (1968) 1208–1211.
[22] W. Hebel, W. Detavernier, M. Decreton, A contribution to the hydrodynamics of boiling crisis in a forced flow of water, Nucl. Eng. Des. 64 (1981) 443–445.
[23] J. Weisman, B.S. Pei, Prediction of critical heat flux in flow boiling at low qualities, Int. J. Heat Mass Transfer 26 (1983) 1463–1477.
[24] C.H. Lee, I. Mudawar, A mechanistic critical heat flux model for subcooled flow boiling based on local bulk flow conditions, Int. J. Multiphase Flow 14 (1988) 711–728.
[25] J.E. Galloway, I. Mudawar, CHF mechanism in flow boiling from a short heated wall-part 1. Examination of near-wall conditions with the aid of photomicrography and high-speed video imaging, Int. J. Heat Mass Transfer 36 (1993) 2511–2526.
[26] J.E. Galloway, I. Mudawar, CHF mechanism in flow boiling from a short heated wall-part 2. Theoretical CHF model, Int. J. Heat Mass Transfer 36 (1993) 2527–2540.
[27] J.C. Sturgis, I. Mudawar, Critical heat flux in a long, rectangular channel subjected to onesided heating – I. Flow visualization, Int. J. Heat Mass Transfer 42 (1999) 1835–1847.
[28] J.C. Sturgis, I. Mudawar, Critical heat flux in a long, rectangular channel subjected to onesided heating – II. Analysis of critical heat flux data, Int. J. Heat Mass Transfer 42 (1999) 1849–1862.
[29] L. Wojtan, R. Revellin, J.R. Thome, Investigation of saturated critical heat flux in a single uniformly heated microchannel, Exp. Therm. Fluid Sci. 30 (2006) 765–774.
[30] D. Del Col, S. Bortolin, Investigation of dryout during flow boiling in a single microchannel under non-uniform axial heat flux, Int. J. Therm. Sci. 57 (2012) 25–36.
[31] S.M. Kim, I. Mudawar, Universal approach to predicting saturated flow boiling heat transfer in mini/micro-channels – Part I. Dryout incipience quality, Int. J. Heat Mass Transfer 64 (2013) 1226–1238.
[32] Y. Katto, General features of CHF of forced convection boiling in uniformly heated rectangular channels, Int. J. Heat Mass Transfer 24 (1981) 1413–1419.
[33] C. Martín-Callizo, Flow boiling heat transfer in single vertical channel of small diameter (Ph.D. thesis), Royal Institute of Technology, Sweden, 2010.
[34] R. Ali, B. Palm, Dryout characteristics during flow boiling of R134a in vertical circular minichannels, Int. J. Heat Mass Transfer 54 (2011) 2434–2445.
[35] W.P. Baek, S.H. Chang, KAIST CHF data, Personal communication, Korea Advanced Institute of Science and Technology, Taejon, South Korea, 1997.
[36] G.M. Roach Jr., S.I. Abdel-Kahlik, S.M. Ghiaasiaan, M.F. Dowling, S.M. Jeter, Low-flow critical heat flux in heated microchannels, Nucl. Sci. Eng. 131 (1999) 411–425.
[37] K.M. Becker, Burnout measurements in vertical round tubes, effect of diameter, AE-TPM-RL-1260, Aktiebolaget Atomenergi, Stockholm, Sweden, 1970.
[38] W. Yu, D.M. France, M.W. Wambsganss, J.R. Hull, Two-phase pressure drop, boiling heat transfer, and critical heat flux to water in a small-diameter horizontal tube, Int. J. Multiphase Flow 28 (2002) 927–941.
[39] C.R. Kharangate, I. Mudawar, M.M. Hasan, Experimental and theoretical study of critical heat flux in vertical upflow with inlet vapor void, Int. J. Heat Mass Transfer 55 (2012) 360–374.
[40] C. Konishi, I. Mudawar, M.M. Hasan, Investigation of localized dryout versus CHF in saturated flow boiling, Int. J. Heat Mass Transfer 67 (2013) 131–146.
[41] G. Guglielmini, E. Nannei, On the effect of heating wall thickness on pool boiling burnout, Int. J. Heat Mass Transfer 19 (1976) 1073–1075.
[42] H. Zhang, I. Mudawar, M.M. Hasan, Flow boiling CHF in microgravity, Int. J. Heat Mass Transfer 48 (2005) 3107–3118.
[43] H.S. Lee, H. Merte, Spherical vapor bubble growth in uniformly superheated liquids, Int. J. Heat Mass Transfer 39 (1996) 2427–2447.
[44] C.R. Class, J.R. DeHaan, M. Piccone, R.B. Cost, Boiling heat transfer to liquid hydrogen from flat surfaces, in: K.D. Timmerhaus (Ed.), Advances Cryogenic Engineering, vol. 5, Plenum Press, New York, NY, 1960.

[45] P.M. Githinji, R.H. Sabersky, Some effects of orientation of the heating surface in nucleate boiling, J. Heat Transfer – Trans. ASME 85 (1963) 379.
[46] W.R. Marcus, D. Dropkin, The effect of surface configuration on nucleate boiling heat transfer, Int. J. Heat Mass Transfer 6 (1963) 863–867.
[47] L.T. Chen, Heat transfer to pool-boiling Freon from inclined heating plate, Lett. Heat Mass Transfer 5 (1978) 111–120.
[48] K. Nishikawa, Y. Fujita, S. Uchida, S., H. Ohta, Effect of heating surface orientation on nucleate boiling heat transfer, in: Y. Mori, W.J. Yang (Eds.), Proc. ASME–JSME Thermal Engineering Joint Conf., vol. 1, Honolulu. HI, 1983, pp. 129–136.
[49] V. Kumar, M. Prasad, M.K. Verma, N.S. Garg, Effect of inclination on pool boiling heat transfer from a flat plate, Indian Chem. Eng. 32 (1990) 61–64.
[50] N. Zuber, M. Tribus, J.W. Westwater, The hydrodynamic crisis in pool boiling of saturated and subcooled liquids, in: Int. Developments Heat Transfer: Proc. Int. Heat Transfer Conf., Boulder, CO, 1961, pp. 230–236.
[51] I. Mudawar, A.H. Howard, C.O. Gersey, An analytical model for near-saturated pool boiling CHF on vertical surfaces, Int. J. Heat Mass Transfer 40 (1997) 2327–2339.
[52] A.H. Howard, I. Mudawar, Orientation effects on pool boiling CHF and modeling of CHF for near-vertical surfaces, Int. J. Heat Mass Transfer 42 (1999) 1665–1688.
[53] R.J. Simoneau, F.F. Simon, A visual study of velocity and buoyancy effects on boiling nitrogen, NASA Tech Note TN D-3354, 1966.
[54] K. Mishima, H. Nishihara, The effect of flow direction and magnitude on CHF for low pressure water in thin rectangular channels, Nucl. Eng. Des. 86 (1985) 165–181.
[55] C.O. Gersey, I. Mudawar, Effects of heater length and orientation on the trigger mechanism for near-saturated flow boiling CHF – I. Photographic and statistical characterization of the near-wall interfacial features, Int. J. Heat Mass Transfer 38 (1995) 629–642.
[56] C.O. Gersey, I. Mudawar, Effects of heater length and orientation on the trigger mechanism for near-saturated flow boiling CHF – II. CHF model, Int. J. Heat Mass Transfer 38 (1985) 643–654.
[57] H. Zhang, I. Mudawar, M.M. Hasan, Experimental assessment of the effects of body force, surface tension force, and inertia on flow boiling CHF, Int. J. Heat Mass Transfer 45 (2002) 4079–4095.
[58] H. Zhang, I. Mudawar, M.M. Hasan, Experimental and theoretical study of orientation effects on flow boiling CHF, Int. J. Heat Mass Transfer 45 (2002) 4463–4478.
[59] H. Zhang, I. Mudawar, M.M. Hasan, Investigation of interfacial behavior during the flow boiling CHF transient, Int. J. Heat Mass Transfer 47 (2004) 1275–1288.
[60] H. Zhang, I. Mudawar, M.M. Hasan, CHF model for subcooled flow boiling in Earth gravity and microgravity, Int. J. Heat Mass Transfer 50 (2007) 4039–4051.
[61] H. Zhang, I. Mudawar, M.M. Hasan, Photographic study of high-flux subcooled flow boiling and critical heat flux, Int. Commun. Heat Mass Transfer 34 (2007) 653–660.
[62] C.R. Kharangate, I. Mudawar, M.M. Hasan, Photographic study and modeling of critical heat flux in horizontal flow boiling with inlet vapor void, Int. J. Heat Mass Transfer 55 (2012) 4154–4168.
[63] C. Konishi, I. Mudawar, M.M. Hasan, Investigation of the influence of orientation on critical heat flux for flow boiling with two-phase inlet, Int. J. Heat Mass Transfer 61 (2013) 176–190.
[64] C. Konishi, I. Mudawar, M.M. Hasan, Criteria for negating the influence of gravity on flow boiling critical heat flux with two-phase inlet conditions, Int. J. Heat Mass Transfer 65 (2013) 203–218.
[65] H. Zhang, I. Mudawar, M.M. Hasan, A method for assessing the importance of body force on flow boiling CHF, J. Heat Transfer – Trans. ASME 126 (2004) 161–168.
[66] G.B. Wallis, One-dimensional Two-Phase Flow, McGraw-Hill Book Company, New York, 1969.
[67] H. Lee, I. Park, I. Mudawar, M.M. Hasan, Micro-channel evaporator for space applications – 1. Experimental pressure drop and heat transfer results for different orientations in Earth gravity, Int. J. Heat Mass Transfer 77 (2014) 1213–1230.
[68] H. Lee, I. Park, I. Mudawar, M.M. Hasan, Micro-channel evaporator for space applications – 2. Assessment of predictive tools, Int. J. Heat Mass Transfer 77 (2014) 1231–1249.
[69] Y. Abe, A. Iwasaki, Pool boiling under microgravity, Adv. Space Res. 13 (1993) 165–168.
[70] T. Oka, Y. Abe, Y.H. Mori, A. Nagashima, Pool boiling of *n*-Pentane, CFC-113, and water under reduced gravity: parabolic flight experiments with a transparent heater, J. Heat Transfer – Trans. ASME 117 (1995) 408–417.
[71] T. Oka, Y. Abe, Y.H. Mori, A. Nagashima, Pool boiling heat transfer in microgravity (experiments with CFC-113 and water utilizing a drop shaft facility), JSME Int. J. 39 (1996) 798–807.
[72] H.S. Lee, H. Merte, Hemispherical vapor bubble growth in microgravity: experiments and model, Int. J. Heat Mass Transfer 39 (1996) 2449–2461.
[73] H. Ohta, K. Kawaji, H. Azuma, K. Kawasaki, H. Tamaoki, K. Ohta, S. Okada, S. Yoda, T. Nakamura, TR-1A rocket experiment on nucleate pool boiling heat transfer under microgravity, Heat Transfer Microgravity Syst. ASME HDT 354 (1997) 249–256.
[74] J. Straub, G. Picker, M. Steinbichler, Boiling and bubble dynamics at a small hemispherical heater under microgravity and Earth conditions, University of Tokyo, in: 2nd Japanese–German Symp. Multi-Phase-Flow, Tokyo, Japan, 1997, pp. 169–176.
[75] J. Straub, Microscale boiling heat transfer under 0g and 1g conditions, Int. J. Therm. Sci. 39 (2000) 490–497.
[76] J. Straub, Origin and effect of thermocapillary convection in subcooled boiling. Observations and conclusions from experiments performed at microgravity, Ann. N.Y. Acad. Sci. 974 (2002) 348–363.
[77] H. Ohta, K. Kawasaki, S. Okada, H. Azuma, S. Yoda, T. Nakamura, On the heat transfer mechanisms in microgravity nucleate boiling, Adv. Space Res. 24 (1999) 1325–1330.
[78] Y. Abe, A. Iwasaki, Single and dual vapor bubble experiments in microgravity, in: Proc. Int. Conf. Microgravity Fluid Physics Heat Transfer, Oahu, HI, 1999, pp. 55–61.
[79] J. Kim, J.F. Benton, D. Wisniewski, Pool boiling heat transfer on small heaters: effect of gravity and subcooling, Int. J. Heat Mass Transfer 45 (2002) 3919–3932.
[80] C.D. Henry, J. Kim, A study of the effects of heater size, subcooling, and gravity level on pool boiling heat transfer, Int. J. Heat Fluid Flow 25 (2004) 262–273.
[81] H. Merte, Momentum effects in steady nucleate pool boiling during microgravity, Ann. N.Y. Acad. Sci. 1027 (2004) 196–216.
[82] H. Merte, Some parameter boundaries governing microgravity pool boiling modes, Ann. N.Y. Acad. Sci. 1077 (2006) 629–649.
[83] C. Sodtke, J. Kern, N. Schweizer, P. Stephan, High resolution measurements of wall temperature distribution underneath a single vapour bubble under low gravity conditions, Int. J. Heat Mass Transfer 49 (2006) 1100–1106.
[84] J.F. Zhao, S.X. Wan, G. Liu, Z.D. Li, W.R. Hu, Pool boiling heat transfer in microgravity, Microgravity Sci. Technol. 19 (2007) 135–136.
[85] J.F. Zhao, G. Liu, S.X. Wan, N. Yan, Bubble dynamics in nucleate pool boiling on thin wires in microgravity, Microgravity Sci. Technol. 20 (2008) 81–89.
[86] J.F. Zhao, J. Li, N. Yan, S.F. Wang, Bubble behavior and heat transfer in quasi-steady pool boiling in microgravity, Microgravity Sci. Technol. 21 (2009) 175–183.
[87] R. Raj, J. Kim, J. McQuillen, Subcooled pool boiling in variable gravity environments, J. Heat Transfer – Trans. ASME 131 (2009) 1–10.
[88] O. Kannengieser, C. Colin, W. Bergez, Pool boiling with non-condensable gas in microgravity: results of a sounding rocket experiment, Microgravity Sci. Technol. 22 (2010) 447–454.
[89] Y.F. Xue, J.F. Zhao, J.J. Wei, J. Li, D. Guo, S.X. Wan, Experimental study of nucleate pool boiling of FC-72 on smooth surface under microgravity, Microgravity Sci. Technol. 23 (Suppl. 1) (2011) S75–S85.
[90] R. Raj, J. Kim, J. McQuillen, Pool boiling heat transfer on the International space station: experimental results and model verification, J. Heat Transfer – Trans. ASME 134 (2012) 1–14.
[91] V.K. Dhir, G.R. Warrier, E. Aktinol, D.F. Chao, J. Eggers, W. Sheredy, W. Booth, Nucleate pool boiling experiments (NPBX) on the international space station, Microgravity Sci. Technol. 24 (2012) 307–325.
[92] R.R. Souza, J.C. Passos, E.M. Cardoso, Confined and unconfined nucleate boiling under terrestrial and microgravity conditions, Appl. Therm. Eng. 51 (2013) 1290–1296.
[93] G. Son, V.K. Dhir, N. Ramanuju, Dynamics and heat transfer associated with a single bubble during nucleate boiling on a horizontal surface, J. Heat Transfer – Trans. ASME 121 (1999) 623–631.
[94] B.N. Antar, Gas–liquid, two phase flow dynamics in low gravity, in: 27th AIAA Dynamics Conf., New Orleans, LA, 1996.
[95] H. Ohta, A. Baba, K. Gabriel, Review of existing research on microgravity boiling and two-phase flow, future experiments on the international space station, Ann. N.Y. Acad. Sci. 974 (2002) 410–427.
[96] G.P. Celata, Flow boiling heat transfer in microgravity: recent progress, Microgravity Sci. Technol. 19 (2007) 13–17.
[97] G.P. Celata, G. Zummo, Flow boiling heat transfer in microgravity: recent progress, Multiphase Sci. Technol. 21 (2009) 187–212.
[98] J.F. Zhao, Two-phase flow and pool boiling heat transfer in microgravity, Int. J. Multiphase Flow 36 (2010) 135–143.
[99] P. Di Marco, Influence of force fields and flow patterns on boiling heat transfer performance: a review, J. Heat Transfer – Trans. ASME 134 (2012) 1–15.
[100] H. Ohta, S. Baba, Boiling experiments under microgravity conditions, Exp. Heat Transfer 26 (2013) 266–295.
[101] C. Baldassari, M. Marengo, Flow boiling in microchannels and microgravity, Prog. Energy Combust. Sci. 39 (2013) 1–36.
[102] D.B. Hepner, C.D. King, J.W. Littles, Zero gravity experiments in two-phase fluids flow regimes, in: ASME Intersociety Conf. Environmental Systems, San Francisco, CA, 1975.
[103] L. Zhao, K.S. Rezkallah, Gas–liquid flow patterns at microgravity, Int. J. Multiphase Flow 19 (1993) 751–763.
[104] B. Choi, T. Fujii, H. Asano, K. Sugimoto, A study of gas–liquid two-phase flow in a horizontal tube under microgravity, Ann. N.Y. Acad. Sci. 974 (2002) 316–327.
[105] A.E. Dukler, J.A. Fabre, J.B. McQuillen, R. Vernon, Gas–liquid flow at microgravity conditions: flow patterns and their transitions, Int. J. Multiphase Flow 14 (1988) 389–400.
[106] W.S. Bousman, Studies of two-phase gas–liquid flow in microgravity (Ph.D. thesis), University of Houston, TX, 1994.
[107] W.S. Bousman, J.B. McQuillen, Characterization of annular two-phase gas–liquid flows in microgravity, in: Proc. 2nd Microgravity Fluid Physics Conf., Cleveland, OH, 1994, pp. 227–232.

[108] W.S. Bousman, J.B. McQuillen, L.C. Witte, Gas–liquid flow patterns in microgravity: effects of tube diameter, liquid viscosity and surface tension, Int. J. Multiphase Flow 22 (1996) 1035–1053.
[109] C. Colin, J. Fabre, A.E. Dukler, Gas–liquid flow at microgravity conditions – I. Dispersed bubble and slug flow, Int. J. Multiphase Flow 17 (1991) 533–544.
[110] C. Colin, A. Kamp, J. Fabre, Influence of gravity on void distribution in two-phase gas–liquid flow in pipe, Adv. Space Res. 13 (1993) 141–145.
[111] C. Colin, J. Fabre, Gas–liquid pipe flow under microgravity conditions: influence of tube diameter on flow patterns and pressure drops, Adv. Space Res. 16 (1995) 137–142.
[112] C. Colin, J. Fabre, J. McQuillen, Bubble and slug flow at microgravity conditions: state of knowledge and open questions, Chem. Eng. Commun. 141–142 (1996) 155–173.
[113] C. Colin, J. Fabre, A. Kamp, Turbulent bubble flow in pipe under gravity and microgravity conditions, J. Fluid Mech. 711 (2012) 469–515.
[114] D. Lee, Thermohydraulic and flow regime analysis for condensing two-phase flow in a microgravity environment (Ph.D. thesis), Texas A&M University, TX, 1987.
[115] D. Lee, F.R. Best, N. McGraw, Microgravity two-phase flow regime modeling, in: Proc. 3rd Nuclear Thermal Hydraulics Winter Meeting, Los Angeles, CA, 1987.
[116] T.R. Reinarts, Adiabatic two phase flow regime data and modeling for zero and reduced (horizontal flow) acceleration fields (Ph.D. thesis), Texas A&M University, TX, 1993.
[117] C.S. Huckerby, K.S. Rezkallah, Flow pattern observations in two-phase gas–liquid flow in a straight tube under normal and microgravity conditions, AIChE Symp. Ser. 88 (1992) 139–147.
[118] R. Rite, K.S. Rezkallah, Heat transfer in two-phase flow through a circular tube at reduced gravity, J. Thermophys. Heat Transfer 8 (1994) 702–708.
[119] J.F. Zhao, W.R. Hu, Slug to annular flow transition of microgravity two-phase flow, Int. J. Multiphase Flow 26 (2000) 1295–1304.
[120] S.S. Jayawardena, V. Balakotaiah, L.C. Witte, Flow pattern transition maps for microgravity two-phase flows, AIChE J. 43 (1997) 1637–1640.
[121] A.M. Shephard, C. Kurwitz, F.R. Best, Microgravity bubbly-to-slug flow regime transition theory and modeling, Microgravity Sci. Technol. 25 (2013) 161–177.
[122] L. Zhao, K.S. Rezkallah, Pressure drop in gas–liquid flow at microgravity conditions, Int. J. Multiphase Flow 21 (1995) 837–849.
[123] R.W. Lockhart, R.C. Martinelli, Proposed correlation of data for isothermal two-phase, two-component flow in pipes, Chem. Eng. Prog. 45 (1949) 39–48.
[124] I. Chen, R. Downing, E.G. Keshock, M. Al-Sharif, Measurements and correlation of two-phase pressure drop under microgravity conditions, J. Thermophys. Heat Transfer 5 (1991) 514–523.
[125] J.F. Zhao, H. Lin, J.C. Xie, W.R. Hu, Pressure drop of bubbly two-phase flow in a square channel at reduced gravity, Adv. Space Res. 29 (2002) 681–686.
[126] C.J. Feldmanis, Pressure and temperature changes in closed loop forced convection boiling and condensing processes under zero gravity conditions, in: Annual Technical Meeting Proceedings, Institute of Environmental Sciences, 1966.
[127] S.S. Papell, An instability effect on two-phase heat transfer for subcooled water flowing under conditions of zero gravity, American Rocket Society 17th Annual Meeting and Space Flight Exposition, 1962.
[128] S.S. Papell, An instability effect on two-phase heat transfer for subcooled water flowing under conditions of zero gravity, NASA Tech Note TN D-2259, 1964.
[129] M. Misawa, An experimental and analytical investigation of flow boiling heat transfer under microgravity conditions (Ph.D. thesis), University of Florida, 1993.
[130] M. Saito, N. Yamaoka, K. Miyazaki, M. Kinoshita, Y. Abe, Boiling two-phase flow under microgravity, Nucl. Eng. Des. 146 (1994) 451–461.
[131] H. Ohta, Experiments on microgravity boiling heat transfer by using transparent heaters, Nucl. Eng. Des. 175 (1997) 167–180.
[132] Y. Ma, J.N. Chung, An experimental study of critical heat flux (CHF) in microgravity forced-convection boiling, Int. J. Multiphase Flow 27 (2001) 1753–1767.
[133] D.T. Westheimer, G.P. Peterson, Visualization of flow boiling in an annular heat exchanger under microgravity conditions, J. Thermophys. Heat Transfer 15 (2001) 333–339.
[134] G.P. Celata, M. Cumo, M. Gervasi, G. Zummo, Flow pattern analysis of flow boiling in microgravity, Multiphase Sci. Technol. 19 (2007) 183–210.
[135] S. Luciani, D. Brutin, C. Le Niliot, O. Rahli, L. Tadrist, Flow boiling in minichannels under normal, hyper-, and microgravity: local heat transfer analysis using inverse methods, J. Heat Transfer – Trans. ASME 130 (2008) 1–13.
[136] C. Baltis, G.P. Celata, M. Cumo, L. Saraceno, G. Zummo, Gravity influence on heat transfer rate in flow boiling, Multiphase Sci. Technol. 24 (2012) 203–213.
[137] D. Brutin, V.S. Ajaev, L. Tadrist, Pressure drop and void fraction during flow boiling in rectangular minichannels in weightlessness, Appl. Therm. Eng. 51 (2013) 1317–1327.
[138] M. Narcy, E. De Malmazet, C. Colin, Flow boiling in straight heated tubes under microgravity conditions, in: Proc. 8th Int. Conf. Multiphase Flow, Jeju, Korea, 2013.
[139] G.P. Celata, M. Cumo, M. Gervasi, G. Zummo, Quenching experiments inside 6.0 mm tube at reduced gravity, Int. J. Heat Mass Transfer 52 (2009) 2807–2814.
[140] G.P. Celata, M. Cumo, F. D'Annibale, L. Saraceno, G. Zummo, Rewetting velocity in quenching at reduced gravity, Int. J. Therm. Sci. 49 (2010) 1567–1575.
[141] S. Luciani, D. Brutin, C. Le Niliot, O. Rahli, Boiling heat transfer in a vertical microchannel: local estimation during flow boiling with a non intrusive method, Multiphase Sci. Technol. 21 (2009) 297–328.